JOURNAL OF PETROLOGY | VOLUME 46 | NUMBER 7 | PAGES 1345–1366 | 2005 | doi:10.1093/petrology/egi018

Crustal Evolution of Island-Arc Ultramafic Magma: Galmoenan Pyroxenite–Dunite Plutonic Complex, Koryak Highland (Far East Russia)

V. G. BATANOVA[1,2]*, A. N. PERTSEV[3], V. S. KAMENETSKY[1,4], A. A. ARISKIN[2], A. G. MOCHALOV[5] AND A. V. SOBOLEV[1,2]

[1]MAX-PLANCK-INSTITUT FÜR CHEMIE, ABT. GEOCHEMIE, POSTFACH 3060, 55020 MAINZ, GERMANY

[2]VERNADSKII INSTITUTE OF GEOCHEMISTRY AND ANALYTICAL CHEMISTRY, RUSSIAN ACADEMY OF SCIENCES, KOSYGIN STR. 19, 117975, MOSCOW, RUSSIA

[3]INSTITUTE OF ORE DEPOSITS GEOLOGY, PETROGRAPHY, MINERALOGY AND GEOCHEMISTRY, STAROMONETNYI, 35, MOSCOW, 109017 RUSSIA

[4]SCHOOL OF EARTH SCIENCES AND CENTRE FOR ORE DEPOSIT RESEARCH, UNIVERSITY OF TASMANIA, HOBART, TAS. 7001, AUSTRALIA

[5]INSTITUTE OF PRECAMBRIAN GEOLOGY AND GEOCHRONOLOGY (IGGD RAS), MAKAROV NAB. 2, ST. PETERSBURG, 199034, RUSSIA

RECEIVED OCTOBER 17, 2003; ACCEPTED JANUARY 26, 2005
ADVANCE ACCESS PUBLICATION FEBRUARY 25, 2005

Alaskan-type platinum-bearing plutons and potassium-enriched mafic to ultramafic volcanic rocks are temporally and spatially associated within the Late Cretaceous–Paleocene Achaivayam–Valaginskii intra-oceanic palaeo-arc system, allochthonously present in the Koryak Highland and Kamchatka Peninsula (Far East Russia). The compositions of the parental magmas to the Alaskan-type complexes are estimated using the Galmoenan plutonic complex as an example. This complex, composed of dunites, pyroxenites and minor gabbros, is the largest (~20 km^3) in the system and the best studied owing to associated platinum placer deposits. The compositions of the principal mineral phases in the Galmoenan intrusive rocks [olivine ($Fo_{79–92}$), clinopyroxene (1–3·5 wt % Al_2O_3, 0·1–0·5 wt % TiO_2), and Cr-spinel (5–15 wt % Al_2O_3 and 0·3–0·7 wt % TiO_2)] are typical of liquidus assemblages in primitive island-arc magmas in intra-oceanic settings, and closely resemble the mineral compositions in the Achaivayam–Valaginskii ultramafic volcanic rocks. The temporal and spatial association of intrusive and extrusive units, and the similarity of their mineral compositions, suggest that both suites were formed from similar parental magmas. The composition of the parental magma for the Galmoenan plutonic rocks is estimated using previously reported data for the Achaivayam–Valaginskii ultramafic volcanic rocks and phenocryst-hosted melt inclusions. Quantitative simulation of crystallization of the parental magma in the Galmoenan magma chamber shows that the compositions of the cumulate units are best modelled by fractional crystallization with periodic magma replenishment. The model calculations reproduce well the observed mineral assemblages and the trace element abundances in clinopyroxene. Based upon the estimated composition of the parental magmas and their mantle source, we consider that fluxing of a highly refractory mantle wedge (similar to the source of boninites) by chlorine-rich aqueous fluids is primarily responsible for both high degrees of partial melting and the geochemical characteristics of the magmas, including their enrichment in platinum-group elements.

KEY WORDS: *subduction; platinum-group elements; clinopyroxene; trace elements; fractional crystallization; Alaskan-type plutons*

*Corresponding author. Telephone: +49-6131-305570. Fax: +49-6131-371051. E-mail: batanova@mpch-mainz.mpg.de

INTRODUCTION

Alaskan-type plutonic complexes were recognized in SE Alaska as a distinct class of intrusions in the 1960s, based on their tectonic setting, composition, internal structure and mineralization (Noble & Taylor, 1960; Taylor & Noble, 1960). In addition to the type locality, similar intrusions have been documented in convergent plate margin settings worldwide—in British Columbia (e.g. Nixon *et al.*, 1990), Oregon (Gray *et al.*, 1986), Venezuela (Murray, 1972), New South Wales, Australia (Johan *et al.*, 1989), Southland, New Zealand (Spandler *et al.*, 2000, 2003), the Ural Mountains (Taylor, 1967) and the Koryak Highland, Northern Kamchatka, Russia (Batanova, 1991; Batanova & Astrakhantsev, 1992, 1994). Alaskan-type plutons are often concentrically zoned and composed (from core to margin) of dunite, wehrlite, olivine clinopyroxenite and hornblende clinopyroxenite, and minor gabbro (Himmelberg & Loney, 1995). The most important characteristic of these intrusive ultramafic rocks is a primary magmatic enrichment in minerals containing platinum-group elements (PGE) with the Pt–Fe alloys (isoferroplatinum) dominating the assemblage (e.g. Slansky *et al.*, 1991; Cabri *et al.*, 1996).

It has been proposed that Alaskan-type intrusions are cumulates derived from the crystallization of hydrous mafic and ultramafic magmas (e.g. Murray, 1972; Irvine, 1974; Himmelberg & Loney, 1995; Helmy & El Mahallawi, 2003). However, the composition and crystallization history of such magmas remain controversial. Irvine (1973, 1974) argued for fractionation of alkaline ultramafic parental magmas (ankaramite) based on the study of subduction-related, K-enriched magnesian rocks from the Juneau area (Alaska). Later research established the origin of the parental magmas of the Alaskan intrusives in a supra-subduction zone tectonic setting, and suggested a subalkaline, orthopyroxene-normative composition (e.g. Nixon *et al.*, 1990; Kepezhinskas *et al.*, 1993; Sha, 1995). In a recent review, Himmelberg & Loney (1995) advocated fractional crystallization of a H_2O-saturated subalkaline island-arc basalt magma for the origin of Alaskan-type complexes based on comparison of their chemical and mineral compositions and the compositions of clinopyroxenite and gabbro xenoliths in the Aleutian arc lavas.

The true nature of the magmas parental to Alaskan-type intrusions and their crystallization paths remains a petrological challenge, particularly in relation to the specific enrichment of these magmas in PGE. Several approaches are used to estimate the compositions of magmas parental to mafic–ultramafic intrusives. Some qualitative methods use the compositions of cumulate minerals, their relative abundances and the order of crystallization (e.g. Thy *et al.*, 1989). Other semi-quantitative methods are based on the use of compositions of chilled margins and aphyric sills and dykes (Hoover, 1989; Greenwood *et al.*, 1990), the compositions of individual minerals and crystal–melt partition coefficients (e.g. Ross & Elthon, 1993), and melt inclusion studies (Batanova *et al.*, 1996; Spandler *et al.*, 2000). An alternative approach to constrain the parental magma compositions of the plutonic rocks is the study of spatially and temporally associated volcanic units, as suggested by Irvine (1973). Based on age and Sr–Nd isotope data, Tistl *et al.* (1994) proposed that spatially associated Alaskan-type ultramafic intrusions and high-K primitive basalts in the Western Cordillera of Colombia are genetically related. However, the chemical and physical parameters of crystal fractionation and accumulation in this case were not quantitatively constrained.

In this study we estimate the compositions of the magmas parental to the Alaskan-type complexes that are widespread in the Kamchatka–Koryak Highland region (NE Russia) using the Galmoenan plutonic complex as an example. This intrusive complex is typical of a regional palaeo island-arc system, formed in the Late Cretaceous–Paleocene (Astrakhantsev *et al.*, 1991; Batanova & Astrakhantsev, 1992, 1994; Kepezhinskas *et al.*, 1993), and is well studied because of associated platinum placer deposits (Mochalov *et al.*, 2002; Nazimova *et al.*, 2003). An important component of the same magmatic palaeosystem is primitive ultramafic volcanic rocks (pillow lavas and dykes), which are highly enriched in large-ion lithophile elements (LILE; Sobolev *et al.*, 1989; Kamenetsky *et al.*, 1995). The occurrence of an extrusive series in close temporal and spatial association with the intrusive complexes is used in this study for the quantitative reconstruction of the composition of the Galmoenan parental magmas. The COMAGMAT 3.5 phase equilibria model (Ariskin *et al.*, 1993; Ariskin, 1999) is applied to constrain the crystallization sequence and mechanisms responsible for the origin of the substantial volumes of ultramafic cumulates, including dunites.

BACKGROUND TO THE GEOLOGY OF THE AREA

The Kamchatka Peninsula and the Koryak Highland form part of the Mesozoic–Cenozoic active continental margin of NE Asia (Fig. 1), where different continental and subduction-related magmatic, sedimentary and metamorphic terranes have been thrust over Late Crataceous–Eocene continental-derived turbidite formations (Konstantinovskaia, 2001, and references therein). One of these terranes, the Achaivayam–Valaginskii Terrane (AVT), includes a number of suites formed in an intra-oceanic arc setting in the Late Cretaceous–Paleocene, and accreted into their current position during the Paleocene–Miocene (Zinkevich & Tsukanov, 1992;

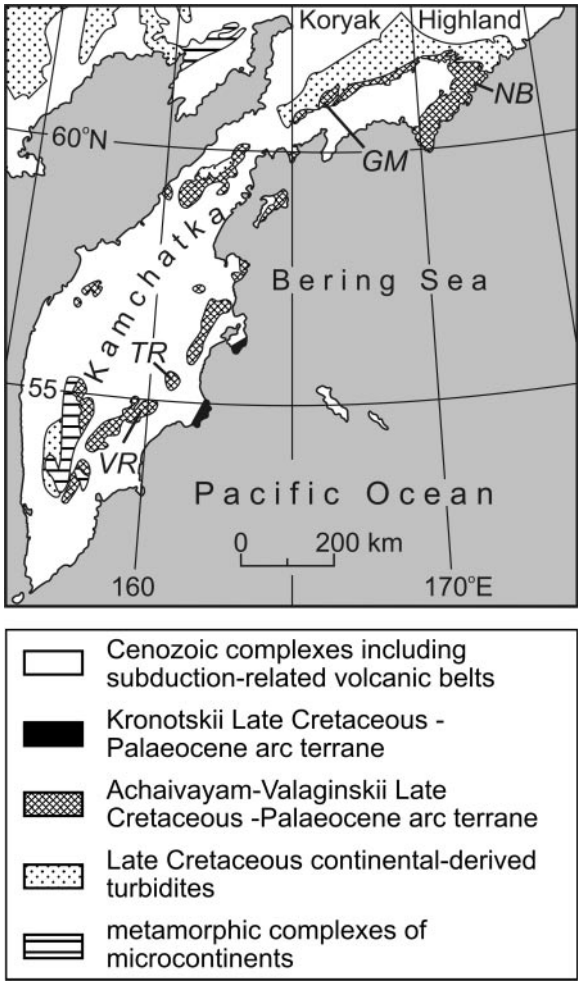

Fig. 1. Map showing the geographical position of the allochthonous complexes of the Achaivayam–Valaginskii palaeo-arc system in the Kamchatka Peninsula and South Koryak Highland. Simplified from Shapiro (1995) and Konstantinovskaia (2001). GM, Galmoenan complex; NB, Natalia Bay; TR, Tumrok Range; VR, Valaginskii Range.

Konstantinovskaia, 2001; Kovalenko, 2001). The basement of the AVT is composed of Albian to Late Campanian, interbedded mid-ocean ridge basalt (MORB)-type volcanic rocks, radiolarian cherts, red jaspers and hyaloclastites, covered by volcaniclastic rocks and lavas of Late Campanian to Paleocene age with strong island-arc geochemical affinities (Astrakhantsev *et al.*, 1987; Konstantinovskaia *et al.*, 1993; Batanova & Astrakhantsev, 1994). Several suites, varying in composition from tholeiitic to high-K (shoshonitic) basalts, have been recognized among the AVT volcanics (Fedorov, 1990; Magakyan *et al.*, 1993). Ultramafic members of the high-K series (pillow lavas, dykes, sills, and tuffs) are present in several localities in eastern Kamchatka and the southern Koryak Highland (Sobolev *et al.*, 1989; Fedorov, 1990; Zinkevich *et al.*, 1991; Kamenetsky *et al.*, 1995), and are considered to be the most primitive representatives of intra-oceanic island-arc high-K magmas (Kamenetsky *et al.*, 1995).

Spatially and temporally associated with the volcanic complexes within the AVT is a belt of more than 20 intrusive bodies, interpreted to have been emplaced in island-arc crust at different levels (Astrakhantsev *et al.*, 1991; Batanova, 1991; Batanova & Astrakhantsev, 1992, 1994; Kepezhinskas *et al.*, 1993). The Galmoenan complex (14 km × 3 km), located in the southern Koryak Highland (Figs 1 and 2) is one of the largest and best exposed of these intrusions. The host rocks are Albian–Campanian silicified tuffs, argillites and black cherts formed in an ocean-floor environment transitional to an island-arc stage. The intrusive rocks were emplaced before the folding and thrusting of the country rocks, and were significantly affected by the latter processes, resulting in plastic and brittle deformation and formation of a serpentinite mélange. The intrusion is concentrically zoned with dunite in the core, followed by wehrlite, olivine clinopyroxenite, hornblende clinopyroxenite, gabbro, and finally orthopyroxene-bearing quartz hornfels at the contact with the country rocks (Fig. 2; Astrakhantsev *et al.*, 1991; Batanova, 1991; Batanova & Astrakhantsev, 1994). The main lithological units of the Galmoenan complex [which are structurally inverted (Astrakhantsev *et al.*, 1991)] are listed in Table 1 and shown in Fig. 2. A dunite body forms the upper part of the ultramafic section in the present-day structure (sections A–B and C–D in Fig. 2); clinopyroxenite commonly underlies the dunite. Small gabbronorite bodies (clinopyroxenite–hornblendite–gabbro unit, see Fig. 2) form the outermost zones of the complex. Several relatively thick (1–5 m) mafic dykes were found within the dunite, clinopyroxenite and country rocks.

STRUCTURE AND PETROGRAPHY OF THE GALMOENAN COMPLEX

Dunite unit

A thick unit of dunites (650 m) dominates the Galmoenan plutonic complex. The dunite is composed of olivine and Cr-spinel, and characterized by a tectonic fabric produced during high-temperature plastic deformation and recrystallization, coeval with emplacement and later thrusting of the whole complex. Most common is a subhorizontal planar fabric with pronounced foliation of olivine porphyroclasts and relic lenses and layers of coarse-grained polygonal and pegmatoid varieties. The planar structures are sub-parallel to the dunite–clinopyroxenite boundary. A range of microstructures (porphyroclastic, granoblastic and mosaic) reflect different degrees of deformation and recrystallization (e.g. Fig. 3a). Veins of olivine clinopyroxenite (1–10 cm thick)

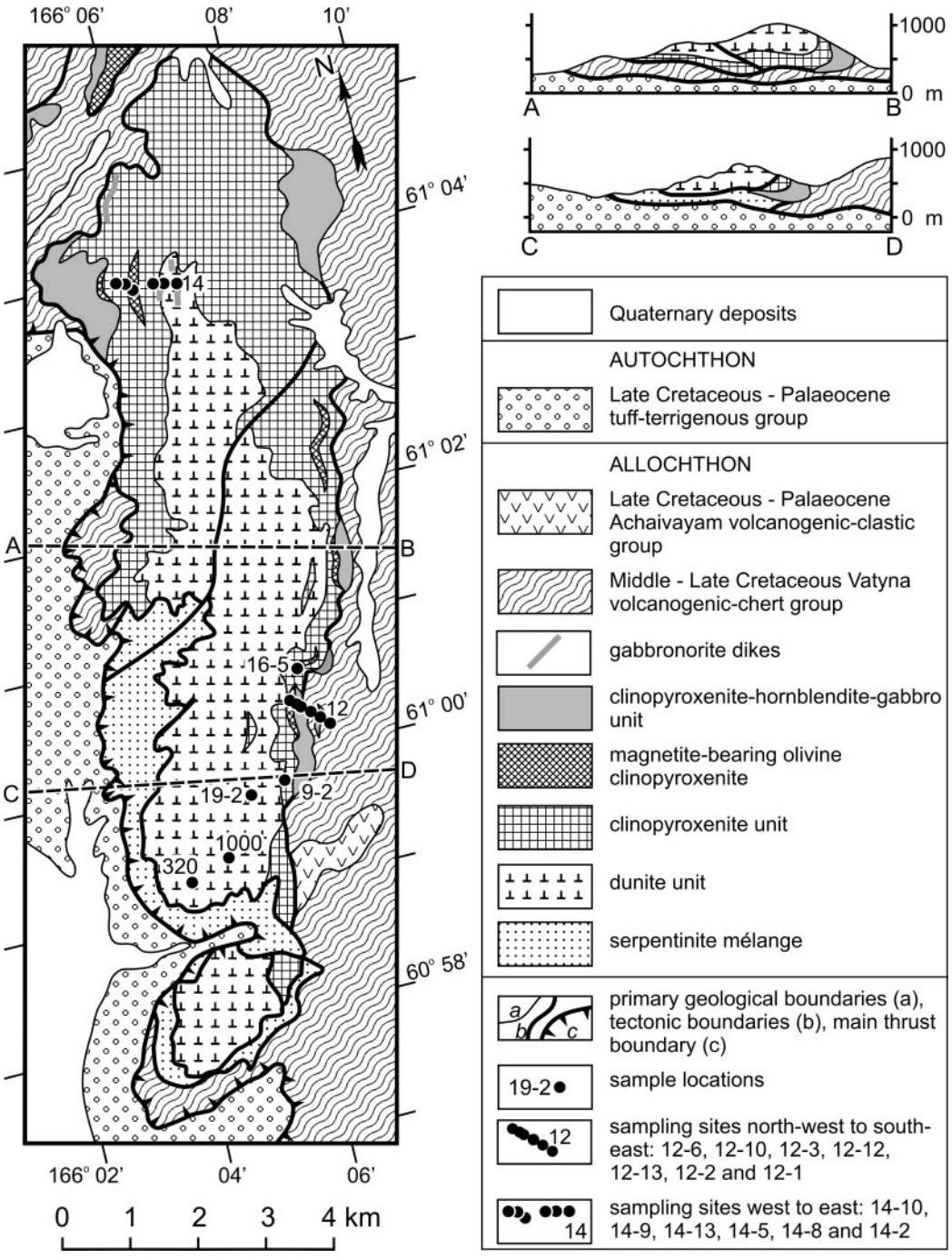

Fig. 2. Detailed geological map and cross-sections of the Galmoenan complex showing sample locations. Modified from Batanova & Astrakhantsev (1994).

are present in the outer part of the dunite unit, close to the contact with the clinopyroxenite.

Dunite–clinopyroxenite transition

The boundary between the dunite and clinopyroxenite units is visually sharp, although clinopyroxene starts to appear in the dunite before the contact. The amount of clinopyroxene gradually increases over a distance of 100–200 m across the contact. Olivine clinopyroxenite veins (up to 1·5 m thick) are abundant in this transition zone. These veins are surrounded by wehrlite and clinopyroxene-bearing dunite (Fig. 3b). Also, several lens-like olivine clinopyroxenite layers up to 10 m thick occur

Table 1: Major rock types and characteristics of Galmoenan massif and AVT ultramafic volcanic rocks

				Spl and Mt		Ol	Cpx
Sample	Rock	Texture	Modal composition (%)	Fe^{3+}/R^{3+}	Cr-no.	Fo	Mg-no.
Dunite unit							
19-2	D	granular	Ol (99); Spl (1)	0·37	75	90·1	—
1000	D	porphyroclastic	Ol (95); Spl (5)	0·23	82	92·2	—
14-5	Cpx D	porphyroclastic	Ol (95); Spl (2–5); Cpx (0–3)	0·26	73	88·9	91·9
320a	Cpxt (vein)	allotriomorphic-	Cpx (100)	—	—	—	93–94
320b	Ol Cpxt (vein)	hypidiomorphic	Cpx (80); Ol (20)	—	—	88·9	91·7
Clinopyroxenite unit							
14-9	Wh	hypidiomorphic–granular	Ol (60); Cpx (40); Spl (<1);	0·37	60	86·9	88·7
			Mt (rim of Spl grain)	0·88	100		
9-2	Ol Cpxt	porphyroclastic	Ol (10; Cpx (90)	—	—	88·0	91·0
14-8	Ol Cpxt	hypidiomorphic–granular	Ol (15); Cpx (85)	—	—	88·4	91·3
14-10	Ol Cpxt	hypidiomorphic–granular	Ol (40); Cpx (60)	—	—	84·1	88·1
1605-1	Mt D (vein)	hypidiomorphic–granular	Ol (85–90); Cr–Ti–Mt (10–15)	0·66	61	85·1	—
Clinopyroxenite–hornblendite–gabbro unit							
14-13	Ol Cpxt	hypidiomorphic–granular	Ol (20); Cpx (80); Mt (<1)	0·91	0·56	81·9	85·4
1605	Ol Cpxt	hypidiomorphic–granular	Ol (10); Cpx (95); Mt (5)	0·94	33	82·0	84·0
12-6	Ol Mt Cpxt	hypidiomorphic–granular	Ol (5); Cpx (90); Mt (5); Phl, Hb (<1)	0·93	43	80·0	83·4
12-2	Pl Cpxt	porphyritic	Ol (3); Cpx (80); Pl (5); Hb (5); Mt (7)	0·90	40	79·0	85* 80†
12-10	Ol Phl Gn	porphyritic	Ol (5); Cpx (60); Opx (10);	0·93	38	81·9	86–87*
			Pl (15); Phl (5); Mt (5)				79–80†
12-12a	Gn	porphyritic	Cpx (45); Opx (10); Pl (30); Hb (3);	0·92	13	—	77·6
			Mt (10); Phl (1); K-Fsp (1)				
12-12b	Gn	porphyritic	Cpx (45); Opx (15); Pl (30);	—	—	—	85·5*
			Mt (10); Phl (<1)				72·2†
12-13a	Nrt	fine-grained equigranular	Opx (25); Pl (65); Mt (10)	0·97	0	—	—
14-12	Hbt	hypidiomorphic	Hb (90); Mt (10); titanite (<1%)	—	—	—	—
AVT ultramafic volcanic rocks							
Tumrok Range							
DAN-51	picrite	porphyritic	Ol and Cpx phenocrysts	0·13–0·37	71·5–80·3	87·2–93·0	82·5–87·8*
		Pl-free matrix					
DAN-57	picrite	porphyritic	Ol (altered) and Cpx phenocrysts	—	—	—	82–88
		altered Pl-free matrix					
Valaginskii Range							
KB-189	picrite	porphyritic	Ol (altered) and Cpx phenocrysts	—	—	—	83–91·8*
		altered Pl-free matrix					
Natalia Bay							
F815-9	picrobasalt	porphyritic	Cpx phenocrysts + altered Pl-free matrix	—	—	—	86–88*
							71–74†

Cpx, clinopyroxene; Ol, olivine; Opx, orthopyroxene; Phl, phlogopite; Pl, plagioclase; Spl, spinel; Hb, hornblende; K-Fsp, K-feldspar; Mt, magnetite; Cpxt, clinopyroxenite; D, dunite; Gn, gabbronorite; Hbt, hornblendite; Nrt, norite; Wh, wehrlite. Cr-number = 100 × Cr/(Cr + Al), mol %; Mg-number = 100 × Mg/(Mg + Fe), mol %; R^{3+} = Cr + Al + Fe^{3+}, mol %.
*Core of mega- or phenocryst.
†Matrix microcryst and/or rim of mega- or phenocryst.

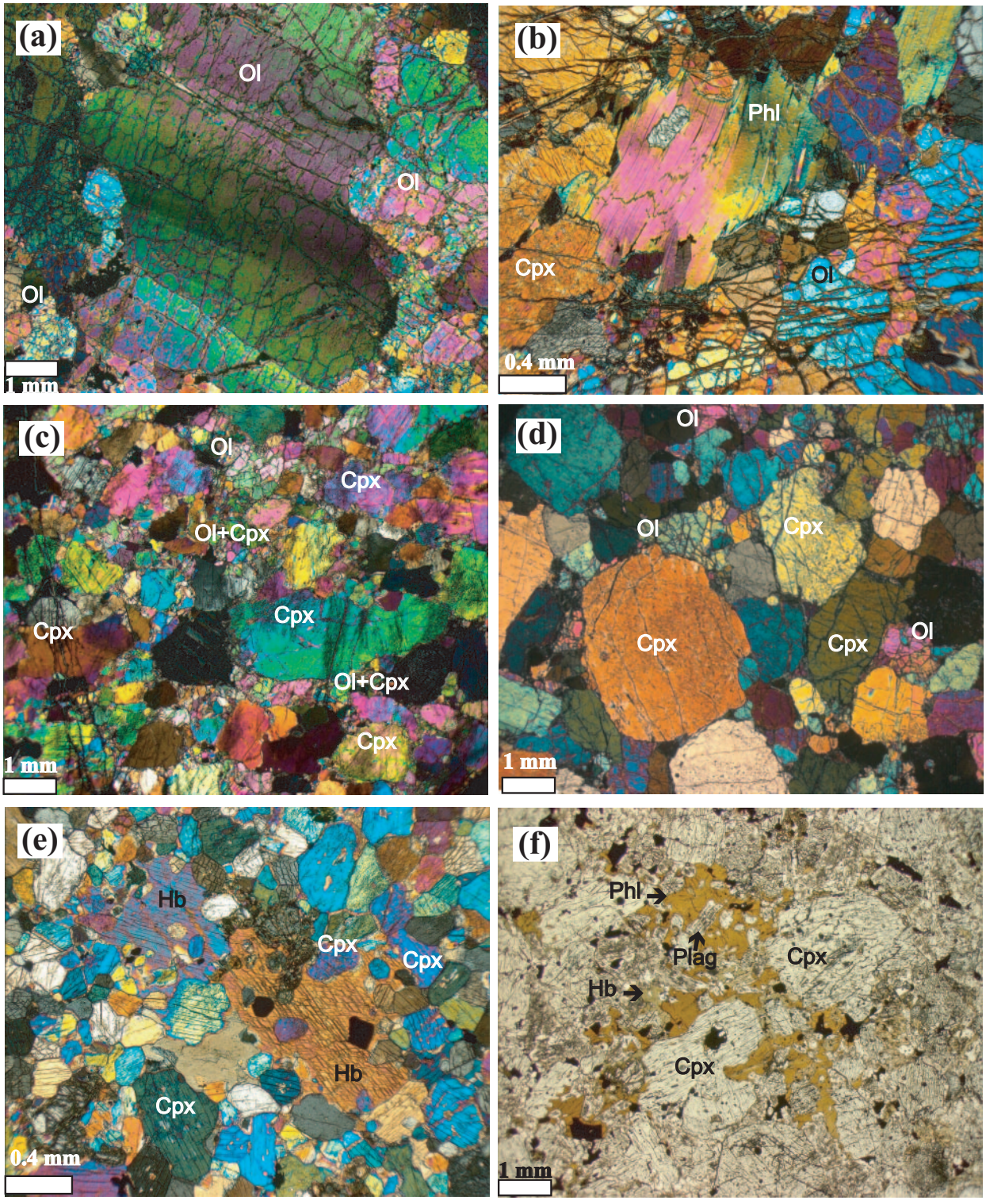

Fig. 3. (a) Porphyroclastic-textured dunite composed of kink-banded olivine porphyroclasts surrounded by olivine neoblasts. (b) Interstitial phlogopite in clinopyroxene-bearing dunite of the transitional dunite–clinopyroxenite zone. (c) Porphyroclastic-textured olivine clinopyroxenite, showing strongly strained clinopyroxene porphyroclasts surrounded by recrystallized olivine and clinopyroxene neoblasts. (d) Non-deformed olivine clinopyroxenite with a cumulate hypidiomorphic–granular texture. (e) Hornblende clinopyroxenite showing poikilitic hornblende crystals. (f) Gabbronorite with poikilitic phlogopite (light brown) and hornblende (green–brown) in interstitial aggregates. (a)–(e) in cross-polarized light; (f) in plane-polarized light.

inside the dunite, above the main dunite–clinopyroxenite transition zone. The transitional zone in the northern part of the complex is characterized by dunite–wehrlite–clinopyroxenite inter-layering (up to 100 m thick). The wehrlite of the dunite–clinopyroxenite transition zone contains abundant spinel, whereas the wehrlite within the clinopyroxenite unit is typically spinel-free. The high-temperature ductile deformation observed in the dunite unit is also characteristic of the rocks in the transition zone, represented by a porphyroclastic textures (Fig. 3c).

Clinopyroxenite unit

The rocks of the clinopyroxenite unit (up to 450 m thick) show no regular stratification, either compositionally or texturally. Bimineralic, coarse- to medium-grained olivine–clinopyroxene rocks are dominant; subordinate magnetite-bearing lithologies with sideronitic textures (xenomorphic magnetite in the matrix cementing clinopyroxene) form layers (up to 50 m thick) throughout the clinopyroxenite unit. There is only a weak planar fabric but local modal layering conforms to the general dunite–clinopyroxenite boundary. Cumulate hypidiomorphic–granular textures are often preserved in the rocks (Fig. 3d), and intracrystalline deformation is developed in mineral grains (sectoral extinction of clinopyroxene, kink-banding in olivine). Clinopyroxene often contains inclusions of phlogopite. Several micro-veins of dunite (up to 5 cm thick) are found within the magnetite-bearing olivine clinopyroxenite.

Clinopyroxenite–hornblendite–gabbro unit

A clinopyroxenite–hornblendite–gabbro unit (up to 500–600 m thick) is located in the outermost zone of the complex. This unit displays a large variety of petrographic and structural features. The clinopyroxenites include hornblende- (Fig. 3e), plagioclase- and magnetite-bearing types, with up to 25% of magnetite in the latter. Close to the contact with the country rocks, the unit is composed of plagioclase- and phlogopite-bearing (± K-feldspar) olivine clinopyroxenite, olivine gabbro, gabbronorite and monzogabbro. These lithologies are characterized by porphyritic textures (Fig. 3f). The contact rocks are aphyric microgabbronorites, micronorites (chilled margin) and orthopyroxene-bearing quartz hornfels (metamorphosed wall rock).

AVT ULTRAMAFIC VOLCANIC ROCKS

Ultramafic volcanic rocks have been previously described from the Valaginskii Range (VR), Tumrok Range (TR) and Natalia Bay (NB) (e.g. Markovsky & Rotman, 1971; Sobolev *et al.*, 1989; Fedorov, 1990; Kamenetsky *et al.*, 1995) (Fig. 1). These rocks are strongly porphyritic picrites (up to 40–75 vol. % of olivine and up to 20 vol. % of clinopyroxene phenocrysts) with a glassy to microcrystalline matrix. The phenocrysts commonly contain inclusions of Cr-spinel and melt. The glassy matrix has a spinifex texture, and is composed of altered glass, clinopyroxene, amphibole, phlogopite and titanomagnetite. Previously studied samples of picrite from TR (DAN-51, DAN-57) and VR (KB-189) and picrobasalt from NB (F815-9) were chosen for comparison with the Galmoenan olivine–clinopyroxene cumulates.

Table 2: Representative analyses of olivine from the Galmoenan massif

Sample:	19-2	1000	14-5	320b	9-2	14-8	14-9	14-10
Rock:	D	D	Cpx D	Ol Cpxt	Ol Cpxt	Ol Cpxt	Wh	Ol Cpxt
SiO_2	40·89	41·81	41·36	40·76	40·75	40·98	40·63	39·92
FeO*	9·11	7·74	10·68	10·58	11·50	11·08	12·14	14·67
MnO	0·19	0·26	0·15	0·24	0·22	0·05	0·09	0·06
MgO	50·29	51·29	48·21	47·45	47·16	47·19	45·27	43·68
NiO	0·15	0·33	0·21	0·22	0·08	0·05	0·10	0·06
CaO	0·06	0·10	0·09	0·17	0·00	0·05	0·01	0·04
Total	100·69	101·53	100·70	99·42	99·71	99·40	98·24	98·43
Fo	90·8	92·2	88·9	88·9	88·0	88·4	86·9	84·1

Sample:	14-13	1605	1605-1	12-6	12-2	12-10
Rock:	Ol Cpxt	Ol Cpxt	Mt D (vein)	Ol Mt Cpxt	Pl Cpxt	Ol Phl Gn
SiO_2	37·79	39·31	39·72	39·25	39·27	39·14
FeO*	17·30	16·87	14·05	19·01	19·26	17·53
MnO	0·36	0·43	0·29	0·28	0·45	0·31
MgO	44·03	43·27	45·08	42·80	40·74	44·50
NiO	0·16	0·09	0·12	0·07	0·13	0·18
CaO	0·05	0·07	0·04	0·04	0·03	0·04
Total	99·69	100·04	99·30	101·45	99·88	101·70
Fo	81·9	82·0	85·1	80·0	79·0	81·9

*Total Fe as FeO.
$Fo = 100 \times (Mg/Mg + Fe^{2+})$.

MINERAL COMPOSITIONS OF THE GALMOENAN COMPLEX AND AVT ULTRAMAFIC VOLCANICS

Olivine

Olivine is present in all ultramafic and most mafic suites of the Galmoenan complex. The olivine is most magnesian in the dunite ($Fo_{90–92}$, Table 2; see Appendix for analytical techniques) and becomes progressively less forsteritic

in the rocks surrounding the dunite core: Fo_{89} in olivine clinopyroxenite and clinopyroxenite veins in dunite, $Fo_{88–84}$ in clinopyroxenite, and Fo_{79} in plagioclase clinopyroxenite and olivine gabbro. Olivine phenocrysts in the AVT ultramafic volcanic rocks range in compositions from Fo_{95} to Fo_{82}, but most samples are $Fo_{92–90}$; several different populations of olivine, varying in CaO content at a given Fo content, have been described (Kamenetsky *et al.*, 1995).

Spinel

Spinel group minerals in the Galmoenan rocks are represented by Cr-spinel (dunite), Cr-magnetite (wehrlite, olivine clinopyroxenite) and magnetite (clinopyroxenite–hornblendite–gabbro unit). Cr-spinel is characterized by high Cr/(Cr + Al) and $Fe^{3+}/(Fe^{3+} + Cr + Al)$ and low Mg-number [$100 \times Mg/(Mg + Fe^{2+})$], TiO_2 and Al_2O_3 (Table 3). Such compositions are typical of spinel in the Alaskan-type complexes and primitive subduction-related volcanic rocks (Figs 4 and 5). Spinel inclusions in olivine from the AVT ultramafic–mafic volcanic rocks are of similar composition, but are more magnesian owing to the higher temperatures of final equilibration with olivine (Figs 4 and 5).

Clinopyroxene

Major elements

Clinopyroxene in all Galmoenan plutonic units is diopsidic in composition (Table 4, Fig. 6) with a high wollastonite component (45–50%), and relatively low Al_2O_3 (1–3·5 wt %) and TiO_2 (0·1–0·5 wt %) (Fig. 7a and b). Similar compositions are reported for clinopyroxene from the studied picrites KB-189, DAN-51, DAN-57 (Fig. 7, Table 5), and from the AVT ultramafic volcanic rocks in general. The Mg-number decreases progressively from 91 in clinopyroxene in the ultramafic cumulates to 78 in clinopyroxene in the mafic rocks (Fig. 7). The increase in Al_2O_3 and TiO_2 with decreasing Mg-number of clinopyroxene (Fig. 7) reflects the crystallization trend in H_2O-bearing subduction-related magmas (Conrad & Kay, 1984; DeBari & Coleman, 1989; Loucks, 1990), and is also typical of Alaskan-type complexes (Himmelberg & Loney, 1995) and of the AVT ultramafic volcanic rocks (Kamenetsky *et al.*, 1995).

Clinopyroxene in the ultramafic units is usually homogeneous, whereas the clinopyroxene phenocrysts in the gabbros and dykes are often zoned. Two generations of clinopyroxene are found in the plagioclase-bearing rocks. The earlier generation comprises large zoned phenocrysts (up to 1 cm) with compositions similar to those in the clinopyroxenite unit (e.g. Mg-number 87–88 mol %). The later generation of smaller grains (0·5–1 mm) is identical in composition (Mg-number 72–80 mol %) to

Table 3: Representative analyses of spinel from the Galmoenan massif

Sample:	19-2	1000	14-5	14-9*	14-9†
Rock:	D	D	Cpx D	Wh	Wh
TiO_2	0·67	0·37	0·76	0·73	0·58
Cr_2O_3	33·97	46·27	40·75	26·88	7·09
Al_2O_3	7·65	6·83	10·14	11·74	0·20
Fe_2O_3	28·03	17·92	18·36	27·74	59·40
FeO	24·81	21·92	23·13	25·55	29·88
MnO	1·44	0·55	0·00	0·00	0·02
MgO	5·02	7·17	7·28	5·05	0·71
NiO	0·06	0·24	0·04	0·08	0·18
Total	101·65	101·27	100·46	97·77	98·06
Fe^{3+}/R^{3+}	0·37	0·23	0·26	0·37	0·88
Cr-no.	75	82	73	60	100

Sample:	14-13	1605	1605-1	12-6	12-2
Rock	Ol Cpxt	Ol Cpxt	Mt D	Ol Mt Cpxt	Pl Cpxt
TiO_2	2·33	2·28	2·06	2·37	2·24
Cr_2O_3	3·20	1·27	13·50	1·82	2·23
Al_2O_3	1·67	1·82	5·81	1·72	2·66
Fe_2O_3	58·41	60·21	45·92	61·76	59·81
FeO	29·94	31·92	29·44	31·85	30·85
MnO	0·18	0·29	0·31	0·26	0·32
MgO	1·76	1·52	2·97	1·30	1·58
NiO	0·13	0·13	0·16	0·08	0·15
Total	97·62	99·44	100·17	101·16	99·84
Fe^{3+}/R^{3+}	0·91	0·94	0·66	0·93	0·90
Cr-no.	56	33	61	43	40

Sample:	12-10	12-12a	12-13a
Rock	Ol Gn	Gn	Nrt
TiO_2	2·84	4·40	0·89
Cr_2O_3	1·73	0·66	0·13
Al_2O_3	1·96	2·97	1·20
Fe_2O_3	60·93	56·77	65·47
FeO	31·13	32·92	32·15
MnO	0·29	0·33	0·36
MgO	2·00	1·80	0·39
NiO	0·18	0·10	0·00
Total	101·06	99·95	100·59
Fe^{3+}/R^{3+}	0·93	0·92	0·97
Cr-no.	38	13	

*Core.
†Rim.
Total iron was determined and Fe_2O_3 and FeO were calculated from spinel stoichiometry.

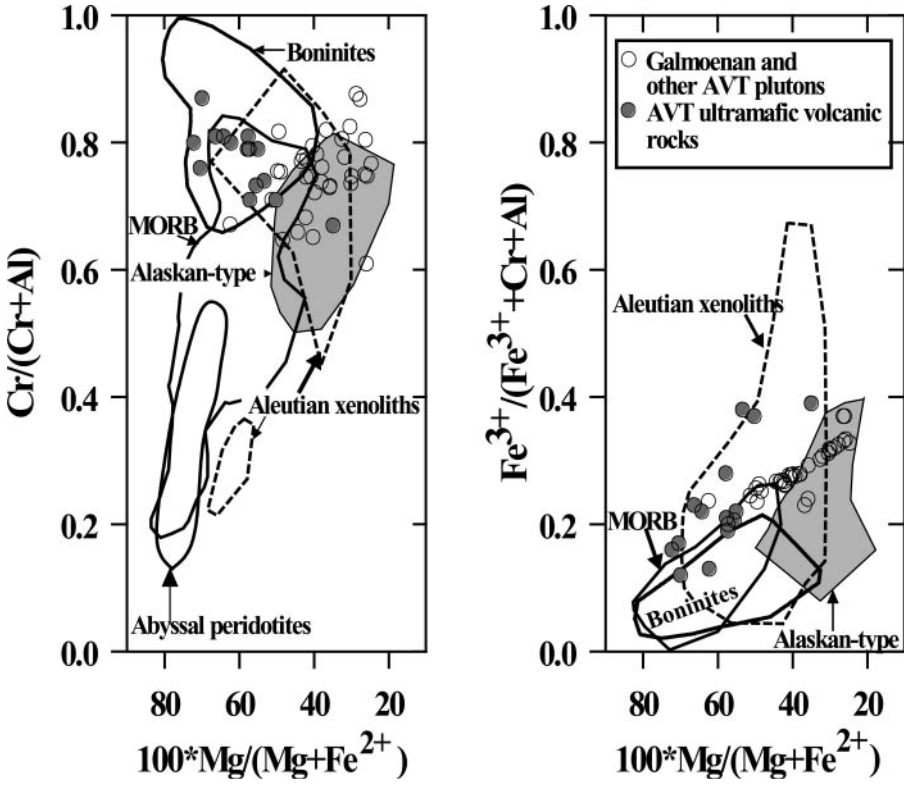

Fig. 4. Cr/(Cr + Al) vs 100 × Mg/(Mg + Fe^{2+}) and Fe^{3+}/(Fe^{3+} + Cr + Al) vs 100 × Mg/(Mg + Fe^{2+}) for Cr-spinel in the Galmoenan complex and AVT ultramafic volcanic rocks (Kamenetsky *et al.*, 1995). The compositional fields of spinel are shown for abyssal peridotites (Dick & Bullen, 1984), boninites and MORB (Barnes & Roeder, 2001), Alaskan-type complexes (Burns, 1985; Himmelberg *et al.*, 1986; Himmelberg & Loney, 1995), Aleutian pyroxenite and gabbro xenoliths (Conrad & Kay, 1984; DeBari *et al.*, 1987; DeBari & Coleman, 1989).

the rims of the phenocrysts of the earlier generation (Table 4). Petrographic observations suggest that the cores of phenocrysts formed prior to plagioclase crystallization, whereas the rims of the phenocrysts and later generation of clinopyroxene crystallized with plagioclase.

Trace elements

Clinopyroxenes from different lithological units of the Galmoenan complex have similar C1-chondrite normalized incompatible trace element patterns (Fig. 8a and b). The characteristic feature of the Galmoenan clinopyroxenes is high Sr and low Zr normalized abundances and relatively flat rare earth element (REE) patterns. The trace element abundances (e.g. Ce_N, Nd_N, Yb_N) increase as Mg-number of the clinopyroxene decreases (Table 4, Fig. 9). The exception is Sr, the concentration of which is nearly constant in clinopyroxene from all lithologies (Fig. 8a and b).

Clinopyroxenes from the olivine clinopyroxenite veins in dunite are characterized by the highest Mg-number and the normalized concentrations of the middle rare earth elements (MREE) and heavy rare earth elements (HREE) similar to those in the clinopyroxenite unit. At relatively constant HREE, La and Ce are highly variable (Fig. 8a). Clinopyroxene in the plagioclase-bearing lithologies is characterized by compositional zoning. Usually the cores of the clinopyroxene phenocrysts have the same trace element patterns as clinopyroxene from the olivine–clinopyroxene cumulates, whereas the rims, as well as grains composing the matrix, are markedly enriched in incompatible elements (Fig. 8b).

Clinopyroxene phenocrysts from the AVT ultramafic volcanic rocks exhibit trace elements patterns closely similar to those observed for clinopyroxene from the Galmoenan plutonic units (Fig. 8c). Clinopyroxenes from the Galmoenan cumulates and the AVT volcanic rocks are well matched in terms of abundances of moderately incompatible elements (Al, Ti, HREE) (Figs 7 and 9), whereas contents of highly incompatible elements (La, Ce, Nd, Sm) are clearly different at a given Mg-number of clinopyroxene. The VR clinopyroxene is most enriched compared with clinopyroxene from TR and NB (consistent with differences in VR and TR whole-rock and melt inclusion compositions; Kamenetsky *et al.*, 1995), whereas the Galmoenan clinopyroxene is compositionally transitional. It is worth noting that clinopyroxene from the olivine clinopyroxenite veins in dunites and

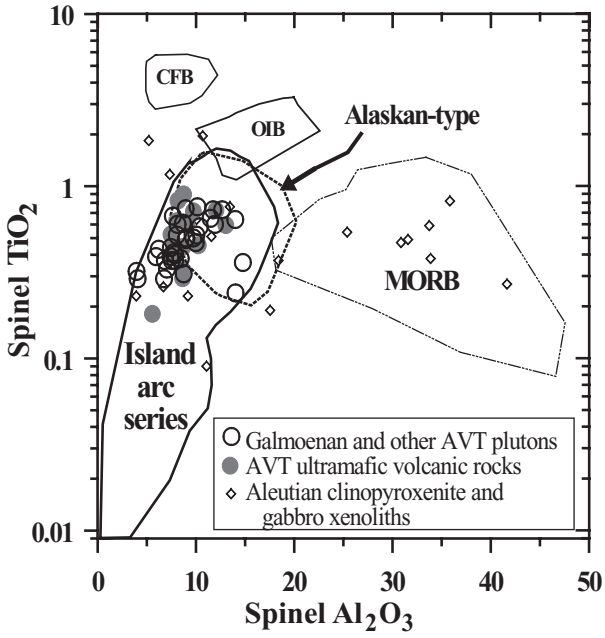

Fig. 5. Comparison of TiO_2 (wt %) and Al_2O_3 (wt %) contents in Cr-spinel in the Galmoenan rocks with compositions of Cr-spinel in volcanic and plutonic complexes from different tectonic environments: AVT ultramafic volcanic rocks (Kamenetsky *et al.*, 1995), Alaskan-type complexes from Alaska (Himmelberg *et al.*, 1986; Himmelberg & Loney, 1995), Aleutian pyroxenite and gabbro xenoliths (Conrad & Kay, 1984; DeBari *et al.*, 1987; DeBari & Coleman, 1989), continental flood basalts (CFB), ocean island basalts (OIB), mid-ocean ridge basalts (MORB), and island-arc series after Kamenetsky *et al.* (2001).

later generation (rims of phenocrysts and matrix grains) clinopyroxene in gabbros is as enriched in most incompatible elements as the VR clinopyroxene (Fig. 9).

Hornblende and phlogopite

Representative compositions of hornblende and phlogopite from the Galmoenan complex are given in Table 6. Hornblende ranging in composition from pargasite to edenite is ubiquitous in the clinopyroxenite–hornblendite–gabbro unit. Phlogopite is present in clinopyroxene-bearing dunites of the dunite–clinopyroxenite transition zone as rare interstitial grains (Fig. 3b), and becomes common in the more evolved (less magnesian) rocks, appearing as inclusions in clinopyroxene. In gabbros, phlogopite is an abundant intercumulus phase, surrounding clinopyroxene and plagioclase (Fig. 3f).

CRYSTALLIZATION MODELLING

Parental melt and input parameters

To model the crystallization processes responsible for the formation of the ultramafic–mafic cumulates we need to define the composition of the parental melt. The inferred genetic link between the Galmoenan plutonic units and the AVT ultramafic volcanic rocks suggests that they could be the products of chemically similar parental magmas. As the composition of the Galmoenan clinopyroxene is most similar to the compositions of volcanic clinopyroxene from TR and NB (Fig. 9) the primary melt defined for the TR ultramafic volcanic rocks (Table 7, composition 1; Kamenetsky *et al.*, 1995) was chosen to represent the parental magma composition of the Galmoenan complex. Accordingly, the Galmoenan parental melt is ultramafic (23·8 wt % MgO), with relatively high H_2O (0·6 wt %), Cl (0·14 wt %) and total alkali contents (2·2 wt %). Its trace element composition was estimated using the compositions of melt inclusions trapped in TR primitive olivine phenocrysts (sample DAN-51; Kamenetsky *et al.*, 1995; Table 7). The degree of oxidation of Fe in the melt $[(Fe^{2+}/Fe^{3+})_L = 3]$ was calculated using the Fe^{2+}/Fe^{3+} of Cr-spinel and the model of Maurel & Maurel (1982).

Preliminary modelling using the COMAGMAT algorithm (Ariskin *et al.*, 1993) shows that the earliest Galmoenan clinopyroxene (Mg-number 90–91) could have crystallized from the model primary melt at a pressure of 3–4 kbar at the given oxidation conditions.

Crystallization models

The ultramafic parental melt (Table 7) is in equilibrium with olivine + Cr-spinel (Kamenetsky *et al.*, 1995). Olivine fractionation was simulated using the PETROLOG 2.1 package (Danyushevsky, 2001) until saturation with clinopyroxene was reached (~17% of olivine fractionation leading to high-Mg basaltic melt, Table 7, composition 2). The simulation of further cotectic crystallization can be performed using either the MELTS algorithm (Ghiorso & Sack, 1995) or COMAGMAT (Ariskin *et al.*, 1993). It has been demonstrated (Yang *et al*, 1996; Slater *et al.*, 2003; Thompson *et al.*, 2003) that both algorithms produce comparable results. However, MELTS tends to overestimate the clinopyroxene crystallization temperature, especially at elevated pressures. On the other hand, COMAGMAT calculates more realistic proportions of cotectic olivine, clinopyroxene and plagioclase, and this explains our preference for COMAGMAT (version 3.5) in the crystallization modelling of the thick (>450 m) olivine–clinopyroxene units of the Galmoenan complex.

Modelling of simple fractional crystallization (Fig. 10) results in a large range of clinopyroxene compositions in the cumulates, but limits crystallization of olivine once clinopyroxene is on the liquidus. Cessation of olivine crystallization is caused by the reaction under given oxidation conditions: olivine + O_2 = pyroxene + magnetite (Ariskin, 2003). Therefore, this model does not explain the presence of olivine in the Galmoenan olivine–clinopyroxene cumulate rocks.

Table 4: The composition of clinopyroxene from the Galmoenan massif

Sample:	14-5	320a	320b	14-9	9-2	14-8	14-10	14-13	12-6	1605	12-2	
Rock:	Cpx D	Cpxt	Ol Cpxt	Wh	Ol Cpxt	Ol Cpxt	Ol Cpxt	Ol Cpxt	Ol Cpxt	Ol Cpxt	Pl Cpxt	
											c	r
Major elements (wt %)												
SiO_2	54·76	53·36	53·55	52·54	53·94	54·23	53·25	51·96	52·96	51·33	53·68	52·91
TiO_2	0·13	0·11	0·19	0·13	0·11	0·11	0·14	0·19	0·24	0·28	0·25	0·38
Cr_2O_3	0·52	0·51	0·61	0·71	0·35	0·38	0·37	0·23	0·11	0·04	0·16	0·11
Al_2O_3	1·17	1·33	1·70	1·31	1·08	1·13	1·39	1·91	2·31	3·07	2·00	3·00
FeO^*	2·61	2·03	2·63	3·70	3·05	2·84	4·06	4·81	5·57	6·13	4·89	6·58
MnO	0·05	0·05	0·04	0·03	0·10	0·10	0·14	0·12	0·15	0·21	0·12	0·26
MgO	16·61	16·84	16·21	16·30	17·25	16·77	16·82	15·75	15·68	15·43	15·69	15·54
CaO	24·18	24·81	24·87	23·25	23·44	23·92	23·61	23·43	22·97	22·52	23·18	21·36
Na_2O	0·31	0·26	0·25	0·22	0·20	0·22	0·22	0·19	0·25	0·22	0·19	0·30
Total	100·34	99·28	100·05	98·19	99·52	99·70	100·00	98·59	100·24	99·23	100·16	100·44
Mg-no.	91·9	93·7	91·7	88·7	91·0	91·3	88·1	85·4	83·4	81·8	85·1	80·8
Trace elements (ppm)												
Ti	696	674	1087	n.d.	692	607	856	1180	1490	n.d.	1300	2390
Sr	163	115	119	n.d.	88	102	104	86	118	n.d.	115	113
Y	3·03	2·28	3·87	n.d.	1·94	1·52	2·65	3·24	5·98	n.d.	4·25	22·7
Zr	1·43	0·79	1·93	n.d.	0·47	0·57	0·91	1·2	3·4	n.d.	2·4	11
La	0·39	0·27	0·99	n.d.	0·092	0·12	0·15	0·14	0·38	n.d.	0·31	0·95
Ce	1·2	0·69	2·8	n.d.	0·41	0·45	0·61	0·56	1·5	n.d.	1·2	4·9
Nd	1·3	0·83	2·7	n.d.	0·69	0·59	0·89	1·1	2·1	n.d.	1·5	7·7
Sm	0·39	0·35	0·82	n.d.	0·32	0·27	0·37	0·46	0·92	n.d.	0·69	3·4
Eu	0·14	0·13	0·29	n.d.	0·11	0·096	0·16	0·21	0·32	n.d.	0·24	0·98
Dy	0·46	0·39	0·74	n.d.	0·39	0·27	0·47	0·58	1·1	n.d.	0·82	4·2
Er	0·38	0·23	0·42	n.d.	0·21	0·13	0·3	0·36	0·68	n.d.	0·5	2·4
Yb	0·28	0·23	0·34	n.d.	0·16	0·13	0·27	0·27	0·55	n.d.	0·42	2·2

Sample:	12-10				12-12a	12-12b	
Rock:	Ol Gn				Gn	Gn	
	c	c	r	m	c	c	m
Major elements (wt %)							
SiO_2	52·71	52·74	50·13	50·42	52·01	52·64	52·66
TiO_2	0·16	0·16	0·68	0·65	0·36	0·12	0·31
Cr_2O_3	0·25	0·30	0·13	0·13	0·08	0·32	0·02
Al_2O_3	1·90	1·53	5·34	5·41	3·26	1·44	1·49
FeO^*	4·70	4·24	6·70	6·89	7·18	4·81	9·43
MnO	0·11	0·14	0·14	0·21	0·24	0·11	0·36
MgO	16·58	16·63	14·57	14·59	14·71	15·94	13·76
CaO	22·66	23·22	22·12	22·35	21·93	23·51	21·35
Na_2O	0·25	0·21	0·48	0·45	0·34	0·19	0·29
Total	99·32	99·17	100·29	101·10	100·11	99·08	99·67
Mg-no.	86·3	87·5	79·5	79·0	78·5	85·5	72·2

Table 4: continued

Sample:	12-10				12-12a	12-12b	
Rock:	Ol Gn				Gn	Gn	
	c	c	r	m	c	c	m
Trace elements (ppm)							
Ti	1100	823	4320	4270	n.d.	n.d.	n.d.
Sr	121	108	71	73	n.d.	n.d.	n.d.
Y	4·65	2·42	24·7	22·7	n.d.	n.d.	n.d.
Zr	3·8	0·97	30	22	n.d.	n.d.	n.d.
La	0·44	0·23	3·6	3·3	n.d.	n.d.	n.d.
Ce	1·5	0·77	13	11	n.d.	n.d.	n.d.
Nd	1·8	1·0	11	9·5	n.d.	n.d.	n.d.
Sm	0·8	0·37	3·7	3·2	n.d.	n.d.	n.d.
Eu	0·28	0·14	1·2	1·1	n.d.	n.d.	n.d.
Dy	0·85	0·52	4·1	3·8	n.d.	n.d.	n.d.
Er	0·52	0·22	2·6	2·5	n.d.	n.d.	n.d.
Yb	0·45	0·21	2·2	2·2	n.d.	n.d.	n.d.

*Total iron as FeO.
c, r, core and rim zone of porphyritic grains respectively; m, grains in the matrix.

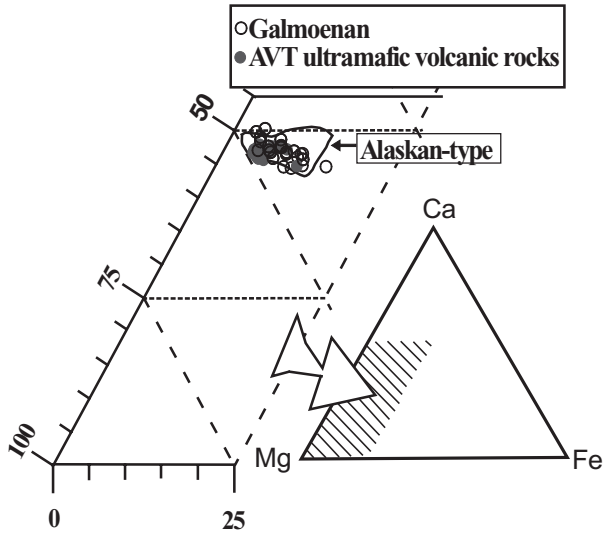

Fig. 6. Clinopyroxene compositions in the Galmoenan complex, AVT ultramafic volcanic rocks and Alaskan-type complexes (Himmelberg *et al.*, 1986; Himmelberg & Loney, 1995).

The second model simulates fractional crystallization (10%) of a high-Mg basalt followed by periodic replenishment of the magma chamber by, and mixing with, small batches (5%) of the parental ultramafic melt (Fig. 11). As expected, the results of this modelling at an early stage of crystallization are not significantly different from simple fractional crystallization (compare Figs 10 and 11). However, after the second cycle of modelled crystallization and replenishment, clinopyroxene follows olivine within every cycle (Fig. 11). This model creates a series of olivine-bearing, clinopyroxene-rich crystallization products with progressively changing Mg-number of olivine (93 to 80) and clinopyroxene (91 to 79). This is consistent with the actual mineral compositions in the Galmoenan cumulates (olivine Fo_{92} to Fo_{79}, clinopyroxene Mg-number 91 to 80). Also this model reproduces well the advanced stages of crystallization [olivine-bearing plagioclase-rich (gabbroic) rocks; see Fig. 11] and describes best the Galmoenan plutonic crystallization trends.

Modelling of the trace element composition of clinopyroxene

A model of fractional crystallization combined with periodic replenishment of new magma was used to simulate the trace element compositions of liquidus clinopyroxene, and thus to test the applicability of the model to the Galmoenan cumulates. We used the clinopyroxene/melt partition coefficients and their temperature dependence as defined by Sobolev *et al.* (1996) for an island-arc H_2O-bearing basaltic melt and low-Al liquidus clinopyroxene compositions (Table 8). The other commonly used clinopyroxene/melt partition coefficients (e.g. Wood & Blundy, 1997) correspond to more Al-rich clinopyroxene and dry conditions and predict much higher values for HREE.

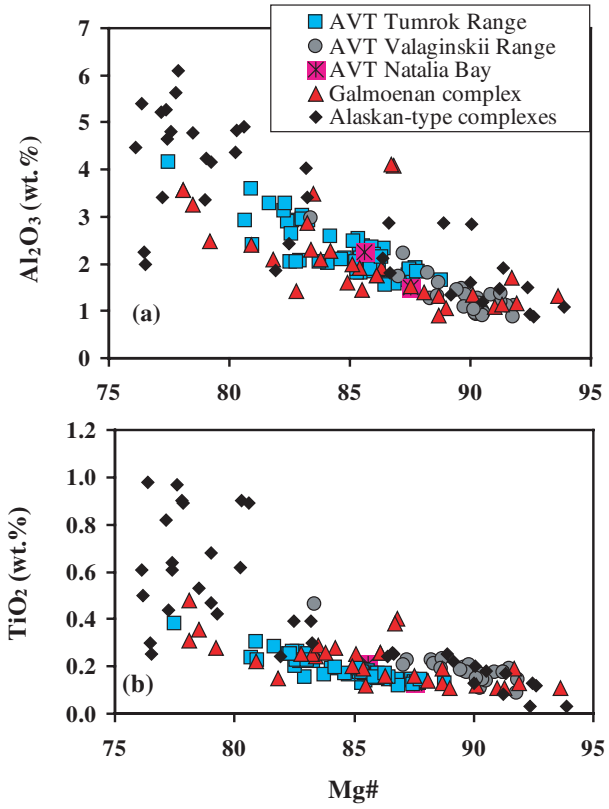

Fig. 7. Relationships between Mg-number and Al_2O_3 (a) and TiO_2 (b) (wt %) in clinopyroxenes from the Galmoenan complex, AVT ultramafic volcanic rocks and Alaskan-type complexes (Himmelberg *et al.*, 1986; Himmelberg & Loney, 1995). Mg-number = 100 × Mg/(Mg + Fe^{2+}) (molecular proportion).

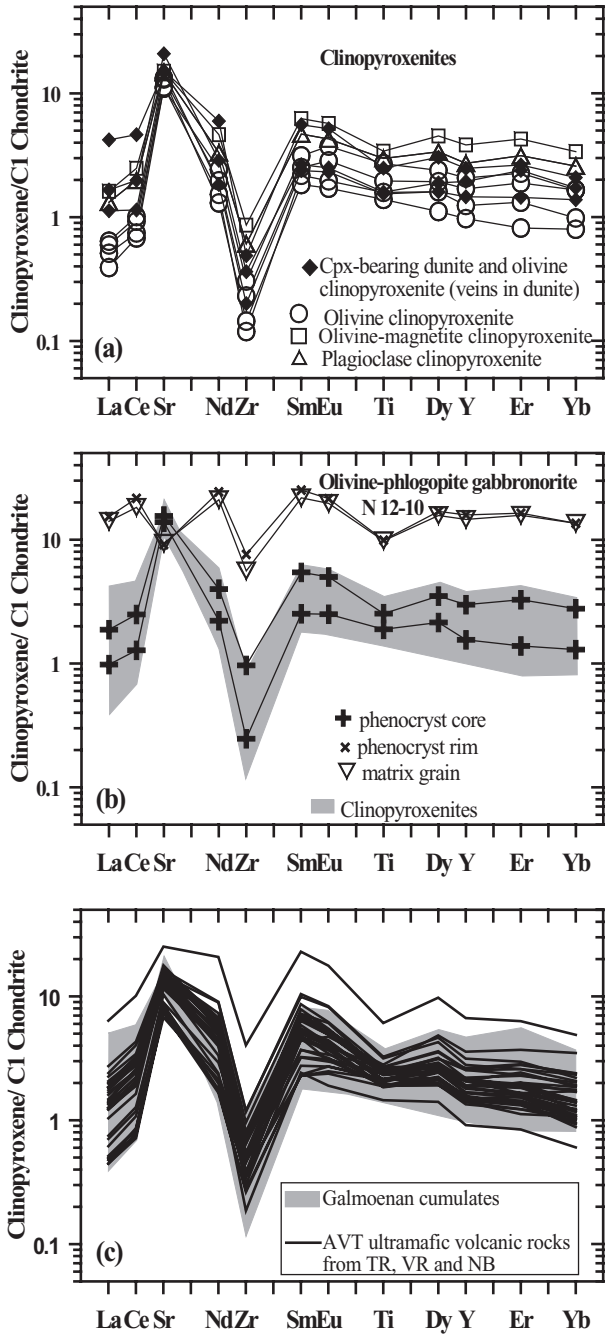

Fig. 8. Chondrite-normalized trace-element abundances in clinopyroxenes from: (a) Galmoenan clinopyroxenite units, (b) a single sample of olivine–phlogopite gabbronorite (N 12-10) and (c) AVT ultramafic volcanic rocks compared with the Galmoenan clinopyroxenite units. Chondrite normalization values are from Anders & Grevesse (1989).

The COMAGMAT algorithm calculates temperatures and modal proportions of liquidus phases for each crystallization increment (1%). This permits calculation of the bulk crystal/melt partitioning of selected trace elements at a given temperature. The crystallization of olivine–clinopyroxene (± magnetite) cumulates suggests that the varying clinopyroxene/melt partition coefficients (Sobolev *et al.*, 1996) and the varying clinopyroxene fraction among the accumulating crystals should principally control the behaviour of Sr, Y and REE, as the abundances of these elements in olivine and spinel are insignificant relative to those in the coexisting clinopyroxene (e.g. Green, 1994; Nielsen *et al.*, 1994). The subsequent crystallization of plagioclase should strongly affect Sr partitioning, whereas REE partitioning remains relatively unchanged (e.g. Bindeman *et al.*, 1998; Lesnov, 2001).

Figure 12 shows that the compositions of clinopyroxene calculated using the model of fractional crystallization with periodic melt replenishment are indeed within the measured range of the Galmoenan clinopyroxene and compositionally analogous clinopyroxene from some AVT ultramafic volcanics (Tumrok Range and Natalia Bay). As we previously pointed out, clinopyroxene from the Valaginskii Range, although similar in HREE abundances, is more enriched in LREE and MREE and thus does not belong to the calculated trend.

Table 5: Representative compositions of clinopyroxene phenocrysts from AVT ultramafic volcanic rocks

Region:	VR	VR	VR	VR	VR	VR	VR	VR	VR
Sample:	KB-189	KB-189	KB-189	KB-189	KB-189	KB-189	KB-189	KB-189	KB-189
Major elements (wt %)									
SiO_2	53·62	52·56	52·14	51·04	53·63	53·12	52·92	53·98	52·93
TiO_2	0·15	0·23	0·23	0·46	0·16	0·18	0·23	0·09	0·18
Cr_2O_3	0·71	0·84	0·73	0·23	0·43	0·77	0·57	0·63	0·66
Al_2O_3	1·12	1·82	2·22	2·96	0·97	1·34	1·59	0·88	1·45
FeO^*	2·78	4·01	4·34	5·59	3·27	3·13	3·86	2·83	3·58
MnO	0·05	0·07	0·09	0·08	0·08	0·06	0·08	0·07	0·06
MgO	17·55	16·86	16·64	15·73	17·56	17·45	16·98	17·73	17·03
CaO	23·64	23·15	23·17	23·37	23·55	23·48	23·38	23·50	23·51
Na_2O	0·21	0·28	0·26	0·31	0·20	0·21	0·22	0·21	0·25
Total	99·83	99·80	99·82	99·77	99·85	99·72	99·82	99·92	99·65
Mg-no.	91·8	88·2	87·2	83·4	90·5	90·9	88·7	91·8	89·5
Trace elements (ppm)									
Sr	114	117	127	197	100	108	116	80·9	139
Y	2·33	3·97	4·91	10·43	2·20	2·45	4·37	1·42	3·23
Zr	1·87	3·77	4·60	15·9	1·39	1·81	4·71	0·73	3·01
La	0·39	0·53	0·64	1·5	0·29	0·33	0·56	0·17	0·49
Ce	1·5	2·1	2·6	6·1	1·2	1·3	2·4	0·71	1·9
Nd	2·3	3·3	4·1	9·4	1·9	2·0	4·0	1·1	2·8
Sm	0·81	1·3	1·5	3·4	0·68	0·74	1·5	0·36	1·0
Eu	0·24	0·35	0·47	0·99	0·17	0·25	0·46	0·11	0·29
Dy	0·53	0·86	1·1	2·4	0·47	0·53	1·0	0·34	0·67
Er	0·22	0·37	0·47	1·0	0·18	0·21	0·41	0·13	0·30
Yb	0·17	0·31	0·36	0·80	0·17	0·20	0·34	0·10	0·24

Region:	TR	TR	TR	TR	TR	TR	NB	NB
Sample:	DAN-51	DAN-51	DAN-51	DAN-51	DAN-57	DAN-57	F815-9	F815-9
Major elements (wt %)								
SiO_2	52·31	52·08	53·52	52·85	52·32	51·48	53·51	54·63
TiO_2	0·13	0·20	0·14	0·16	0·16	0·19	0·21	0·13
Cr_2O_3	0·90	0·18	0·72	0·25	0·43	0·77	0·61	0·51
Al_2O_3	1·91	2·05	1·83	1·85	1·89	2·47	2·25	1·49
FeO^*	4·18	6·16	4·15	4·76	5·12	5·05	4·89	4·19
MnO	0·10	0·14	0·09	0·11	0·13	0·12	0·09	0·11
MgO	16·80	16·29	16·80	16·71	16·68	16·24	16·25	16·42
CaO	22·83	22·28	23·00	22·98	22·37	22·40	24·02	23·66
Na_2O	0·26	0·23	0·20	0·22	0·19	0·24	0·23	0·15
Total	99·41	99·60	99·46	99·89	99·29	98·96	102·04	101·29
Mg-no.	87·7	82·5	87·8	86·2	85·3	85·2	85·6	87·5
Trace elements (ppm)								
Sr	66·5	69·9	65·5	61·1	53·0	57·6	91·7	65·7
Y	3·44	5·58	3·24	2·93	4·12	4·05	3·52	1·81
Zr	1·37	2·57	1·49	1·03	1·81	2·04	1·78	0·67
La	0·12	0·18	0·10	0·11	0·11	0·14	0·19	0·13
Ce	0·50	0·77	0·47	0·45	0·52	0·65	0·80	0·36

Region:	TR	TR	TR	TR	TR	TR	NB	NB
Sample:	DAN-51	DAN-51	DAN-51	DAN-51	DAN-57	DAN-57	F815-9	F815-9
Nd	0·89	1·32	0·80	0·78	0·97	1·05	1·2	0·59
Sm	0·41	0·65	0·34	0·34	0·48	0·54	0·60	0·34
Eu	0·15	0·26	0·14	0·15	0·17	0·19	0·22	0·10
Dy	0·62	1·17	0·62	0·59	0·76	0·88	0·58	0·28
Er	0·36	0·59	0·39	0·32	0·45	0·44	0·36	0·19
Yb	0·33	0·57	0·30	0·30	0·39	0·39	0·31	0·18

*Total iron as FeO.

DISCUSSION AND CONCLUSIONS

The temporal and spatial association of both the Alaskan-type Galmoenan complex and the ultramafic extrusive suites of the Achaivayam–Valaginskii terrane within the same Late Cretaceous–Paleocene intraoceanic island-arc system, allochthonously emplaced in the Koryak Highland and Kamchatka Peninsula in NE Russia, suggests a genetic affinity. The comagmatic nature of the intrusive and extrusive rocks is supported by the composition of their primitive liquidus assemblage—high-Mg olivine, high-Cr and low-Ti spinel, and diopsidic clinopyroxene depleted in Al and Ti (Figs 4–7). This allows us to assume that both suites crystallized from similar parental magmas. In other words, the magmas previously identified as parental to the AVT volcanic rocks (Sobolev *et al.*, 1989; Kamenetsky *et al.*, 1995) could be parental to the cumulate rocks of the Galmoenan complex. These ultramafic melts (19–24 wt % MgO), should be recognized as a new magma type within the island-arc compositional spectrum. Unlike common subduction-related magmas (calc-alkaline, tholeiitic and boninitic series) they are exceptional in having significant enrichment in potassium, chlorine and LILE relative to REE, strongly depleted high-field strength elements of similar incompatibility, and MORB-like neodymium isotope ratios (Kamenetsky *et al.*, 1995). The high potassium contents of the Galmoenan parental magmas are independently supported by the presence of phlogopite in the ultramafic rocks and gabbros and K-feldspar in the gabbros. We note that arc-related high-Mg parental magmas enriched in potassium have also been proposed for at least two other Alaskan-type ultramafic complexes (Irvine, 1973; Tistl *et al.*, 1994).

The parental magma composition, proposed here to be common for the Galmoenan plutonic units and the AVT ultramafic volcanic rocks, is independently substantiated by consideration of the trace element compositions of clinopyroxene from both intrusive and extrusive suites (Figs 8 and 9). First of all, their overall similarity argues for crystallization from compositionally similar parental melts, assuming that the partitioning of trace elements between clinopyroxene and melt was similar in both cases. Second, the calculated melt compositions in equilibrium with clinopyroxene from the Galmoenan cumulates and the AVT ultramafic volcanic rocks show close similarity to the trace element compositions of the inferred parental magmas of the AVT ultramafic volcanic rocks, as represented by olivine-hosted melt inclusions (Fig. 13). This is the most compelling evidence for the formation of the Galmoenan cumulates from ultramafic island-arc magmas, similar to those identified previously for the extrusive sequences of the AVT (Kamenetsky *et al.*, 1995).

The simulation of crystallization in the Galmoenan magma chamber from the parental magma (defined based on the comparison of AVT ultramafic volcanic rocks and their melt inclusions) shows that the compositions of the cumulate units are best modelled by a

Table 6: Representative analyses of hornblende and phlogopite from the Galmoenan massif

Sample:	1605	12-6	12-2	12-10		12-12A	
Rock:	Ol Mt Cpxt	Ol Cpxt	Pl Cpxt	Ol Gn		Gn	
Mineral:	Hb	Phl	Hb	Hb	Phl	Hb	Phl
SiO_2	44·88	39·65	43·51	43·13	38·12	44·12	38·42
TiO_2	1·26	1·93	1·35	1·49	2·23	2·29	3·95
Cr_2O_3	0·09	0·10	0·00	0·00	0·09	0·32	0·15
Al_2O_3	13·28	17·02	11·56	12·70	16·98	11·82	15·98
FeO	9·02	7·19	9·63	9·67	8·62	10·69	10·76
MnO	0·21	0·00	0·15	0·14	0·07	0·09	0·05
MgO	16·26	22·79	15·23	16·14	21·14	14·58	17·70
CaO	12·30	0·04	11·98	12·37	0·01	12·41	0·04
Na_2O	1·71	0·63	2·13	2·36	0·44	1·92	0·49
K_2O	0·36	10·05	0·78	1·17	10·02	0·93	9·07
Total	99·37	99·40	96·32	99·1	97·72	99·17	96·61
Mg-no.	76·3	85·0	73·8	74·8	81·4	70·80	74·6

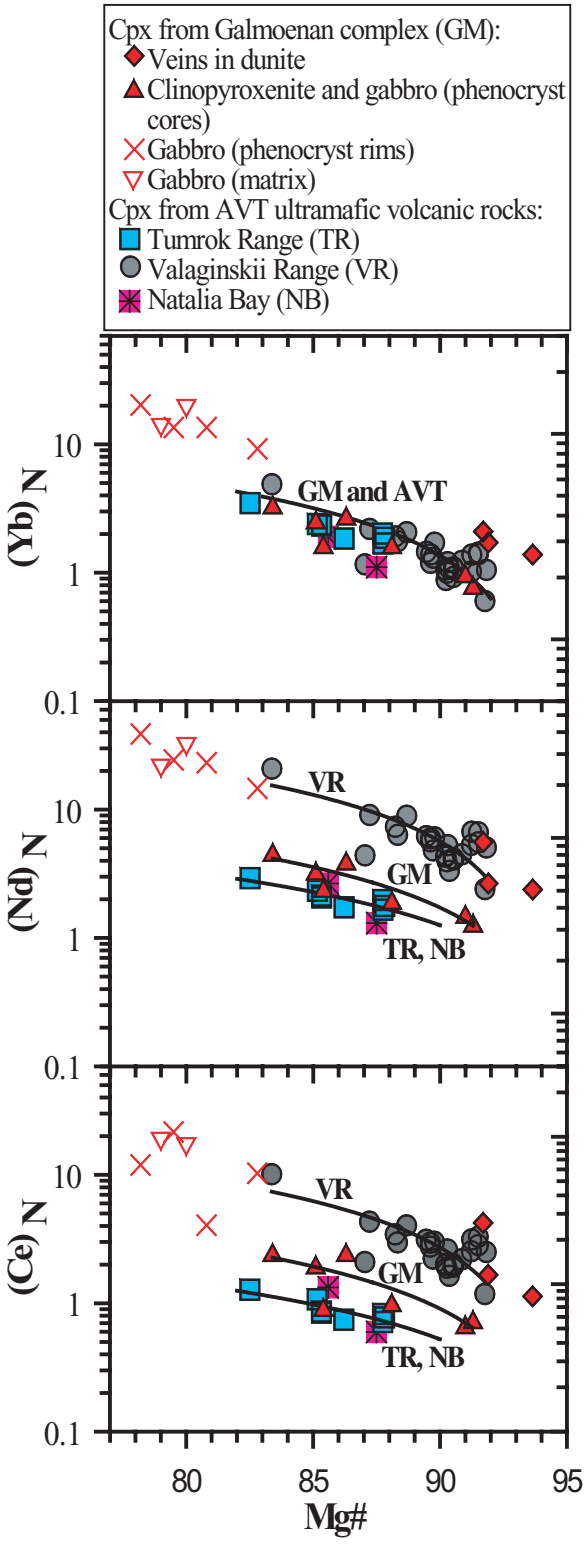

Fig. 9. Relationships between Mg-number and chondrite-normalized Yb, Nd and Ce in clinopyroxene from the Galmoenan complex and AVT (VR, TR and NB) ultramafic volcanic rocks. Chondrite normalization values are from Anders & Grevesse (1989). Mg-number = $100 \times Mg/(Mg + Fe^{2+})$ (molecular proportion).

Table 7: The composition and fractionation of the parental melt

	1	2
Major elements (wt %)		
SiO_2	46·99	47·65
TiO_2	0·29	0·35
Al_2O_3	8·20	9·81
FeO_{tot}	9·22	9·87
MnO	0·12	0·14
MgO	23·80	17·63
CaO	8·71	10·42
Na_2O	1·15	1·38
K_2O	1·06	1·27
P_2O_5	0·20	0·24
H_2O	0·62	0·74
Cl	0·14	0·17
Trace elements (ppm)		
Sr	391	472
Y	7·0	8·4
Zr	14·0	16·9
La	2·49	3·00
Ce	4·99	6·02
Nd	3·37	4·06
Sm	1·14	1·38
Dy	1·44	1·74
Er	0·87	1·04
Yb	0·87	1·04

1, inferred parental melt composition of the Galmoenan intrusive rocks. This composition represents the primary melt previously defined for the AVT (Tumrok Range) ultramafic volcanic rocks (Kamenetsky *et al.*, 1995).
2, melt composition resulting from 17% olivine + spinel fractionation of the parental melt.

process of fractional crystallization with periodic magma replenishment. This provides reasonable explanations for the large amounts of dunite present (~30 wt % of the model parental melt; Fig. 11), the significant interval of co-crystallization of olivine, clinopyroxene and later plagioclase, and also the range of compositions (in terms of Mg-number) of the liquidus mafic minerals.

An additional test for the validity of the crystallization models can be provided by relationships between the Mg-number and incompatible elements in the calculated and actual clinopyroxene compositions (Fig. 12). The model of fractional crystallization with replenishment produces an instantaneous increase in both Mg-number and trace element abundances in the clinopyroxene at each 'episode' of replenishment, and thus approximates the actual compositions of clinopyroxene from clinopyroxenites and gabbros better than simple fractionation

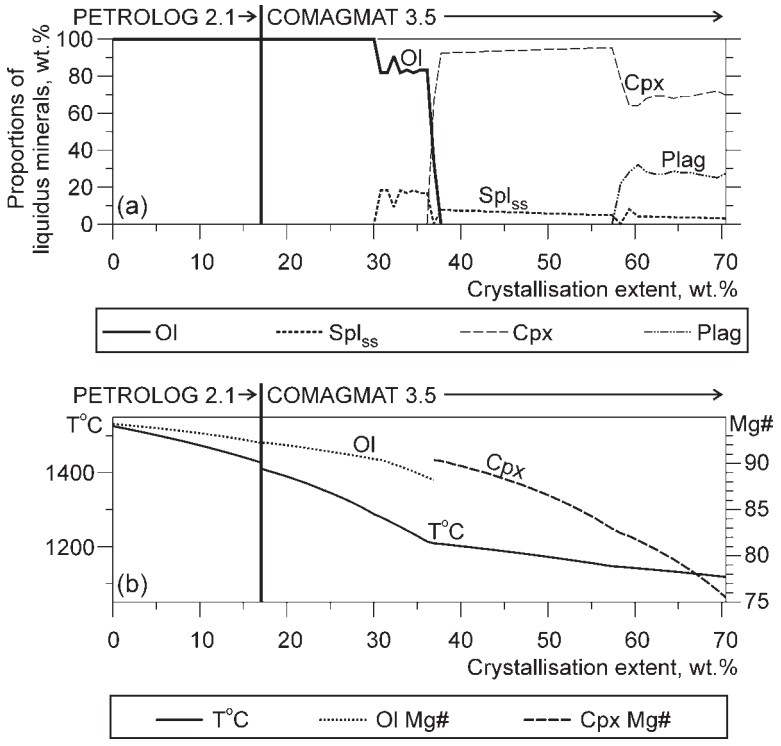

Fig. 10. Modelling of simple fractional crystallization of the ultramafic parental melt. (a) Modal proportions of crystallizing minerals vs extent of crystallization; (b) temperature and Mg-number of olivine and clinopyroxene during progressive crystallization.

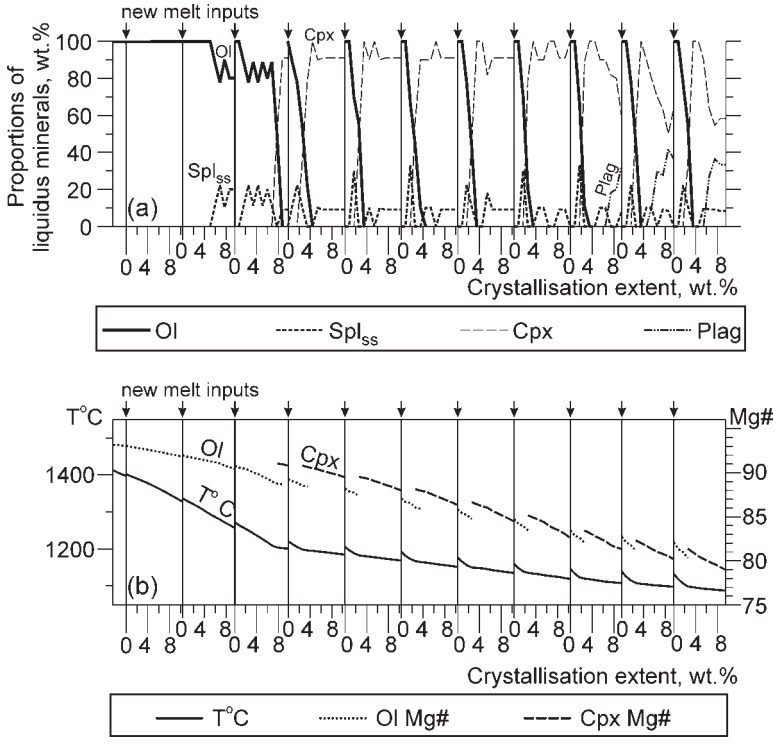

Fig. 11. Modelling of fractional crystallization of the ultramafic parental melt with periodic replenishment. (a) Modal proportions of crystallizing minerals vs extent of crystallization; (b) temperature and Mg-number of olivine and clinopyroxene during progressive crystallization.

Table 8: Clinopyroxene/melt partition coefficients

T(°C):	1204	1150	1100	1078
Mg-no. Cpx:	91·0	86·6	80·7	78·0
La	0·020	0·029	0·042	0·050
Ce	0·037	0·055	0·082	0·099
Sr	0·12	0·083	0·059	0·051
Nd	0·06	0·12	0·22	0·29
Zr	0·027	0·043	0·067	0·083
Sm	0·10	0·19	0·35	0·47
Dy	0·11	0·24	0·54	0·79
Y	0·09	0·23	0·55	0·85
Er	0·10	0·21	0·43	0·61
Yb	0·10	0·20	0·42	0·59

Cpx/melt partition coefficients calculated using the equations of Sobolev *et al.* (1996). Temperature (*T*,°C) and cpx composition (Mg-number) are calculated from the modelling of fractional crystallization with replenishment using the COMAGMAT algorithm.

(Fig. 12). The model curves have the 'sawtooth' shape reflecting the changes in the clinopyroxene composition caused by mixing with the primitive magma. Simple fractional crystallization produces a similar overall trend (decreasing Mg-number with increasing REE); however, the real REE concentrations in clinopyroxene are not modelled well. We thus assume a dominant role of fractional crystallization and replenishment of the magma chamber with small batches of primitive melt. Although the actual variations in composition, mass and frequency of melt injections cannot be quantified, this model reflects the general impact of the refilling on the final crystallization products.

The systematically higher trace element abundances at a given Mg-number in clinopyroxene from the veins in dunites, and in clinopyroxene belonging to later generation (rims of phenocrysts and matrix grains) in the plagioclase-bearing rocks resemble the compositions of clinopyroxene from the Valaginskii Range ultramafic volcanic rocks (Figs 9 and 12). This, taken together with the previously described stronger enrichment in incompatible trace elements of the Valaginskii Range (VR) magmas compared with the Tumrok Range (TR) magmas (Kamenetsky *et al.*, 1995), may argue for a temporal change in the magma composition during plutonic evolution of the Galmoenan magmatic system. In other words, there exists a possibility that the Galmoenan magma chamber initially filled with a TR-type melt was subsequently replenished with more enriched VR-type melts. It has been suggested that the mantle source for the ATV ultramafic magmas was a highly refractory peridotite, fluxed with subduction-derived enriched melts

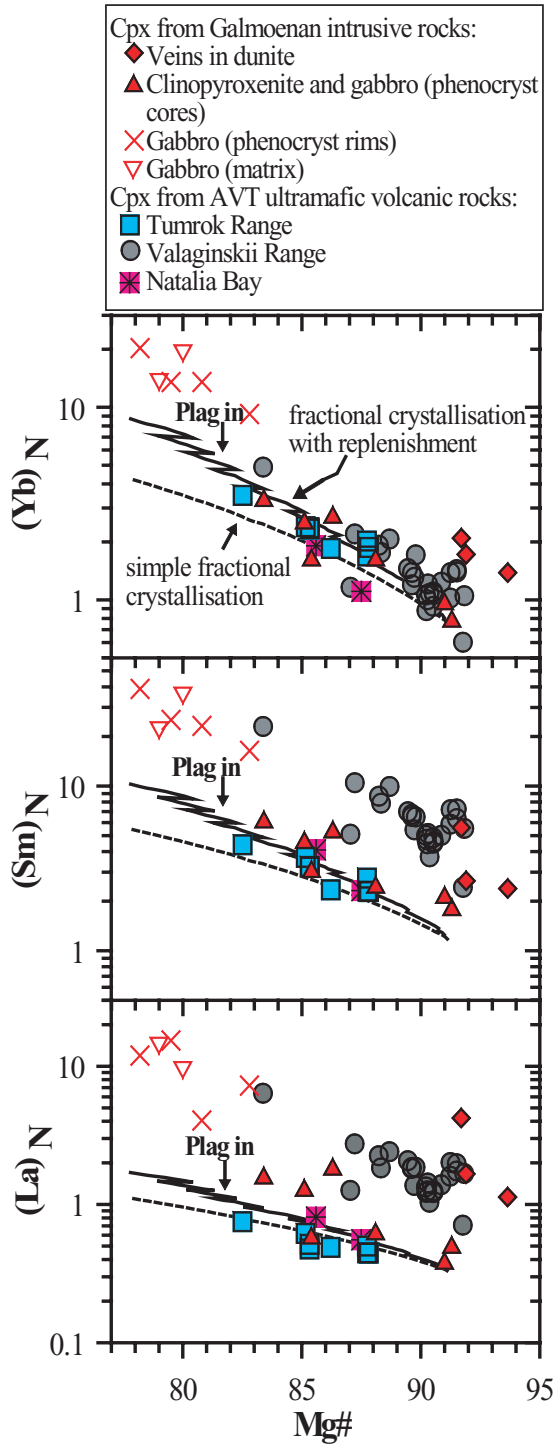

Fig. 12. Comparison between the chondrite-normalized REE (Y, Sm, La) compositions of the Galmoenan and AVT (VR, TR and NB) clinopyroxenes and clinopyroxene compositional trends calculated using the fractional crystallization models in Figs 10 and 11. Calculations were performed using the composition of olivine-hosted melt inclusions as the parental magma (Table 7; Kamenetsky *et al.*, 1995) and the clinopyroxene/melt partition coefficients (Table 8) of Sobolev *et al.* (1996). Chondrite normalization values are from Anders & Grevesse (1989).

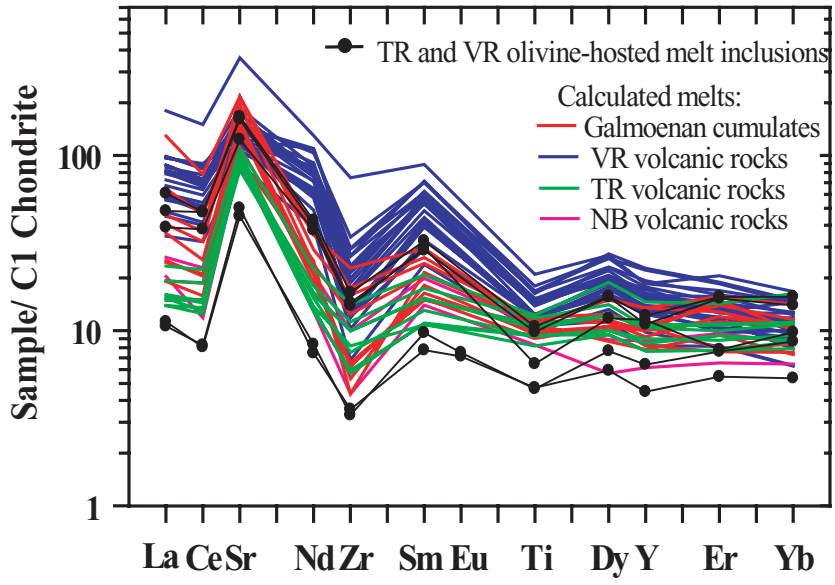

Fig. 13. Chondrite-normalized trace element compositions of hypothetical magmas calculated to be in equilibrium with the clinopyroxene in the Galmoenan complex and AVT (VR, TR and NB) ultramafic volcanic rocks. The compositions of melt inclusions in the AVT olivines (TR and VR) are plotted for comparison. Clinopyroxene/melt partition coefficients are from Sobolev *et al.* (1996). Chondrite normalization values are after Anders & Grevesse (1989).

and fluids at a depth of at least 100 km (Kamenetsky *et al.*, 1995). We speculate that the observed evolution of the Galmoenan magmatic system reflects the change in the subduction-derived components (amount and composition) in the mantle source.

The formation of magmatic platinum-group minerals is a first-order function of the absolute quantity of PGE available in the melt; thus we need to understand the factors responsible for PGE enrichment in magmas. The composition of the mantle source and the conditions of melting are clearly important in constraining the PGE enrichment of the parental magmas forming the Galmoenan and other Alaskan-type intrusive complexes. The mantle source proposed for the Galmoenan parental magmas is a highly refractory peridotite, strongly depleted in 'basaltic' components but subsequently metasomatized by reaction with the trace element enriched fluids and melts. This source could have been 'pre-enriched' in PGE by previous melting episodes. Refractory mantle peridotite (harzburgite) has been proposed as the source of primitive boninite magmas in subduction-related environments (e.g. Hickey & Frey, 1982; Cameron *et al.*, 1983; Crawford *et al.*, 1989; Kamenetsky *et al.*, 2002) and we note that the AVT ultramafic volcanic rocks have a 'boninitic' magma component represented by low-Ca olivine phenocrysts and olivine-hosted clinoenstatite inclusions (Kamenetsky *et al.*, 1995). The origin of the PGE mineralization in the Bushveld and Stillwater igneous complexes has been ascribed to crystallization (in part) from high-Mg boninitic magmas (e.g. Sharpe & Hulbert, 1985; Hatton & Scharpe, 1989; Boudreau *et al.*, 1997). Although the compatible behaviour of the PGE during melting causes progressively increasing PGE abundances in the refractory mantle residue, the preferential extraction of PGE into partial melts of harzburgite requires additional constraints. These can be provided by numerous studies on the role of chlorine-rich aqueous fluids in the redistribution of PGE within their host intrusive rocks (e.g. Boudreau *et al.*, 1986; Hsu *et al.*, 1991; Boudreau, 1993; Fleet & Wu, 1993) and transport at magmatic conditions (Sassani & Shock, 1998). In accord with the conclusions of Willmore *et al.* (2002), and the given high chlorine contents in the AVT parental magmas, we envisage that fluxing of a refractory mantle wedge in a supra-subduction zone tectonic setting by chlorine-rich aqueous fluids is primarily responsible for the formation of PGE-enriched magmas.

ACKNOWLEDGEMENTS

We acknowledge P. Fedorov for providing the picrobasalt sample (F815), and S. Simakin, D. Kuzmin and B. Stoll for help with analytical studies. An anonymous reviewer is thanked for thoughtful comments. We greatly appreciate the editorial handling and insightful reviews by R. J. Arculus and M. Wilson. This work was supported by the Wolfgang Paul Award (Alexander von Humboldt Stiftung, Germany) to A.V.S. V.S.K. acknowledges the Friedrich Wilhelm Bessel Award (Alexander von Humboldt Stiftung, Germany) that provided funding for his stay in Mainz.

REFERENCES

Anders, E. & Grevesse, N. (1989). Abundance of the elements: meteoritic and solar. *Geochimica et Cosmochimica Acta* **53**, 197–214.

Ariskin, A. A. (1999). Phase equilibria modeling in igneous petrology: use of COMAGMAT model for simulating fractionation of ferro-basaltic magmas and the genesis of high-alumina basalt. *Journal of Volcanology and Geothermal Research* **90**, 115–162.

Ariskin, A. A. (2003). The compositional evolution of differentiated liquids from the Skaergaard Layered Series as determined by geochemical thermometry. *Russian Journal of Earth Sciences* **5**, 1–29.

Ariskin, A. A., Frenkel, M. Ya., Barmina, G. S. & Nielsen, R. L. (1993). COMAGMAT: a Fortran program to model magma differentiation processes. *Computers and Geosciences* **19**, 1155–1170.

Astrakhantsev, O. V., Kazimirov, A. D., Krylov, K. A. & Fedorov, P. I. (1987). Tectonics and structure of the Vatyna nappe frontal part (Koryak Highland). *Doklady Akademii Nauk SSSR* **295**, 157–160 (in Russian).

Astrakhantsev, O. V., Batanova, V. G. & Perfiliev, A. S. (1991). Structure of the Galmoenan dunite–clinopyroxenite–gabbro massif (South Koryak Region). *Geotectonics* **25**, 132–144.

Barnes, S. J. & Roeder, P. L. (2001). The range of spinel compositions in terrestrial mafic and ultramafic rocks. *Journal of Petrology* **42**, 2279–2302.

Batanova, V. G. (1991). Mafic–ultramafic intrusive complexes from South Koryakia. Ph.D. thesis, Moscow: Geological Institute RAS, 350 pp. (in Russian).

Batanova, V. G. & Astrakhantsev, O. V. (1992). Tectonic position and origin of zoned mafic–ultramafic plutons of the North Olyutor zone (Koryak upland). *Geotectonics* **26**, 153–165.

Batanova, V. G. & Astrakhantsev, O. V. (1994). Island-arc mafic–ultramafic plutonic complexes of North Kamchatka. In: Ishiwatari, A., Malpas, J. & Ishizuka, H. (eds) *Proceedings of the 29th International Geological Congress, Part D, Circum-Pacific Ophiolites*. Utrecht: VSP, pp. 129–143.

Batanova, V. G., Sobolev, A. V. & Schmincke, H. U. (1996). Parental melts of the intrusive cumulates of the Troodos massif, Cyprus: a study of clinopyroxenes and melt inclusions in plagioclase. *Petrology* **4**, 255–264.

Bindeman, I. N., Davis, A. M. & Drake, M. J. (1998). Ion microprobe study of plagioclase–basalt partition experiments at natural concentration levels of trace elements. *Geochimica et Cosmochimica Acta* **62**, 1175–1193.

Boudreau, A. E. (1993). Chlorine as an exploration guide for the platinum-group elements in layered intrusions. *Journal of Geochemical Exploration* **48**, 21–37.

Boudreau, A. E., Mathez, E. A. & McCallum, I. S. (1986). Halogen geochemistry of the Stillwater and Bushveld complexes—evidence for transport of the platinum-group elements by Cl-rich fluids. *Journal of Petrology* **27**, 967–986.

Boudreau, A. E., Stewart, M. A. & Spivack, A. J. (1997). Stable Cl isotopes and origin of high-Cl magmas of the Stillwater Complex, Montana. *Geology* **25**, 791–794.

Burns, L. E. (1985). The Border Ranges ultramafic and mafic complex, south–central Alaska—cumulate fractionates of island-arc volcanics. *Canadian Journal of Earth Sciences* **22**, 1020–1038.

Cabri, L. J., Harris, D. C. & Weizer, T. W. (1996). Mineralogy and distribution of platinum-group mineral placer deposits of the world. *Exploration and Mining Geology* **5**, 73–167.

Cameron, W. E., McCulloch, M. T. & Walker, D. A. (1983). Boninite petrogenesis: chemical and Nd–Sr isotopic constraints. *Earth and Planetary Science Letters* **65**, 75–89.

Conrad, W. K. & Kay, R. W. (1984). Ultramafic and mafic inclusions from Adak Island—crystallization history, and implications for the nature of primary magmas and crustal evolution in the Aleutian arc. *Journal of Petrology* **25**, 88–125.

Crawford, A. J., Falloon, T. J. & Green, D. H. (1989). Classification, petrogenesis and tectonic setting of boninites. In: Crawford, A. J. (ed.) *Boninites*. London: Unwin Hyman, pp. 1–49.

Danyushevsky, L. V. (2001). The effect of small amounts of H_2O on crystallisation of mid-ocean ridge and backarc basin magmas. *Journal of Volcanology and Geothermal Research* **110**, 265–280.

DeBari, S. M. & Coleman, R. G. (1989). Examination of the deep levels of an island arc: evidence from the Tonsina ultramafic–mafic assemblage, Tonsina, Alaska. *Journal of Geophysical Research* **94**(B4), 4373–4391.

DeBari, S. M., Kay, S. M. & Kay, R. W. (1987). Ultramafic xenoliths from Adagdak volcano, Adak, Aleutian Islands, Alaska—deformed igneous cumulates from the Moho of an island-arc. *Journal of Geology* **95**, 329–341.

Dick, H. J. B. & Bullen, T. (1984). Chromian spinel as a petrogenetic indicator in abyssal and alpine-type peridotites and spatially associated lavas. *Contributions to Mineralogy and Petrology* **86**(1), 54–76.

Fedorov, P. I. (1990). Geochemistry and petrology of Late Cretaceous volcanics in the Koryak Upland. *Geokhimiya* **11**, 1583–1594 (in Russian).

Fleet, M. E. & Wu, T. W. (1993). Volatile transport of platinum-group elements in sulfide–chloride assemblages at 1000°C. *Geochimica et Cosmochimica Acta* **57**, 3519–3531.

Ghiorso, M. S. & Sack, R. O. (1995). Chemical mass transfer in magmatic processes. IV. A revised and internally consistent thermodynamic model for the interpolation and extrapolation of liquid–solid equilibria in magmatic systems at elevated temperatures and pressures. *Contributions to Mineralogy and Petrology* **119**, 197–212.

Gray, F., Page, N. J., Carlson, C. A., Wilson, S. A. & Carlson, R. R. (1986). Platinum-group element geochemistry of zoned ultramafic intrusive suites, Klamath Mountains, California and Oregon. *Economic Geology* **81**, 1252–1260.

Green, T. H. (1994). Experimental studies of trace-element partitioning applicable to igneous petrogenesis—Sedona 16 years later. *Chemical Geology* **117**, 1–36.

Greenwood, R. C., Donaldson, C. H. & Emeleus, C. H. (1990). The contact zone of the Rhum ultrabasic intrusion—evidence of peridotite formation from magnesian magmas. *Journal of the Geological Society, London* **147**, 209–212.

Hatton, C. J. & Scharpe, M. R. (1989). Significance and origin of boninite-like rocks associated with the Bushveld complex. In: Crawford, A. J. (ed.) *Boninites*. Boston, MA: Unwin Hyman, pp. 174–207.

Helmy, H. M. & El Mahallawi, M. M. (2003). Gabbro Akarem mafic–ultramafic complex, Eastern Desert, Egypt: a Late Precambrian analogue of Alaskan-type complexes. *Mineralogy and Petrology* **77**, 85–108.

Hickey, R. L. & Frey, F. A. (1982). Geochemical characteristics of boninite series volcanics: implications for their source. *Geochimica et Cosmochimica Acta* **46**, 2099–2115.

Himmelberg, G. R. & Loney, R. A. (1995). Characteristics and petrogenesis of Alaskan-type ultramafic–mafic intrusions, Southeastern Alaska. *US Geological Survey, Professional Papers* **1564**, 1–47.

Himmelberg G. R., Loney, R. A. & Craig, J. T. (1986). Petrogenesis of the ultramafic complex at the Blashke Islands, Southern Alaska. *US Geological Survey Bulletin* **1662**, 1–14.

Hoover, J. D. (1989). The chilled marginal gabbro and other contact rocks of the Skaergaard Iintrusion. *Journal of Petrology* **30**, 441–476.

Hsu, L. C., Lechler, P. J. & Nelson, J. H. (1991). Hydrothermal solubility of palladium in chloride solutions from 300°C to

700°C—preliminary experimental results. *Economic Geology and the Bulletin of the Society of Economic Geologists* **86**, 422–427.

Irvine, T. N. (1973). Bridget Cove volcanics, Juneau Area, Alaska: possible parental magma of Alaskan-type ultramafic complexes. *Carnegie Institution of Washington, Yearbook* **72**, 478–491.

Irvine, T. N. (1974). *Petrology of the Duke Island Ultramafic Complex, Southern Alaska. Geological Society of America, Memoirs* **138**, 240 pp.

Jarosevich, E. J., Nelen, J. A. & Norberg, J. A. (1980). Reference samples for electron microprobe analysis. *Geostandards Newsletter* **4**, 43–47.

Jochum, K. P., Dingwell, D. B., Rocholl, A., Stoll, B., Hofmann, A. W., Becker, S., *et al.* (2000). The preparation and preliminary characterisation of eight geological MPI-DING reference glasses for in-situ microanalysis. *Geostandards Newsletter* **24**, 87–133.

Johan, Z., Ohnenstetter, M., Slansky, E., Barron, L. M. & Suppel, D. (1989). Platinum mineralization in the Alaskan-type intrusive complexes near Fifield, New South Wales, Australia: 1. Platinum-group minerals in clinopyroxenites of the Kelvin Grove prospect, Owendale Intrusion. *Mineralogy and Petrology* **40**, 289–309.

Kamenetsky, V. S., Sobolev, A. V., Joron, J. L. & Semet, M. P. (1995). Petrology and geochemistry of Cretaceous ultramafic volcanics from Eastern Kamchatka. *Journal of Petrology* **36**, 637–662.

Kamenetsky, V. S., Crawford, A. J. & Meffre, S. (2001). Factors controlling chemistry of magmatic spinel: an empirical study of associated olivine, Cr-spinel and melt inclusions from primitive rocks. *Journal of Petrology* **42**, 655–671.

Kamenetsky, V. S., Sobolev, A. V., Eggins, S. M., Crawford, A. J. & Arculus, R. J. (2002). Olivine-enriched melt inclusions in chromites from a low-Ca boninite, Cape Vogel, Papua New Guinea: evidence for ultramafic primary magma, refractory mantle source and enriched components. *Chemical Geology* **183**, 287–303.

Kepezhinskas, P. K., Reuber, I., Tanaka, H. & Miyashita, S. (1993). Zoned calc-alkaline plutons in Northern Kamchatka, Russia: implications for the crustal growth in magmatic arcs. *Mineralogy and Petrology* **49**, 147–174.

Konstantinovskaia, E. A. (2001). Arc–continent collision and subduction reversal in the Cenozoic evolution of the Northwest Pacific: and example from Kamchatka (NE Russia). *Tectonophysics* **333**, 75–94.

Konstantinovskaia, E. A., Zinkevich, V. P., Tsukanov, N. V. & Garanina, S. A. (1993). Composition and structure of the Upper Cretaceous to Lower Paleogene lithostructural complexes in the Easter Ranges of Kamchatka. In: Puchsharovskii, Yu. M. (ed.) *Accretional Tectonics of the Eastern Kamchatka*. Moscow: Nauka, pp. 59–113 (in Russian).

Kovalenko, D. V. (2001). A model for the tectonic accretion of island-arc terranes in Kamchatka and Southern Koryak highland. *Geotectonics* **35**, 403–418.

Lesnov, F. P. (2001). Geochemistry of rare-earth elements in plagioclase. *Geologiya i Geofizika* **42**, 917–936.

Loucks, R. R. (1990). Discrimination of ophiolitic from nonophiolitic ultramafic–mafic allochthons in orogenic belts by the Al/Ti ratio in clinopyroxene. *Geology* **18**, 346–349.

Magakyan, R., Kolesov, G. M., Romashova, T. V. & Konstantinovskaia, E. A. (1993). Geochemical features of Cretaceous island-arc magmatism of Eastern Kamchatka. In: Puchsharovskii, Yu. M. (ed.) *Accretional Tectonics of the Eastern Kamchatka*. Moscow: Nauka, pp. 114–155 (in Russian).

Markovsky, B. A. & Rotman, V. K. (1971). Geosyncline meimechites of Kamchatka. *Doklady Akademii Nauk SSSR* **196**, 675–678 (in Russian).

Maurel, C. & Maurel, P. (1982). Etude expérimentale de l'équilibre Fe^{2+}–Fe^{3+} dans les spinelles chromifières et les liquides silicates basiques coexistants, à 1 atm. *Comptes Rendus de l'Académie des Sciences* **295**, 209–212.

Mochalov, A. G., Zaitsev, V. P., Pertsev, A. N. & Vlasov, E. A. (2002). Mineralogy and genesis of 'alluvial platinum' from placers of the Southern Koryak Highland (Russia). *Geology of Ore Deposits* **44**, 188–212.

Murray, C. G. (1972). Zoned ultramafic complexes of the Alaskan type: feeder pipes of andesitic volcanoes. *Geological Society of America, Memoirs* **132**, 313–335.

Nazimova, Yu. V., Zaitsev, V. P. & Mochalov, A. G. (2003). Platinum group minerals of the Gal'moenan gabbro–pyroxenite–dunite massif in the southern part of the Koryak Highland (Russia). *Geology of Ore Deposits* **45**, 481–499.

Nielsen, R. L., Forsythe, L. M., Gallaghan, W. E. & Fisk, M. R. (1994). Major and trace element magnetite/melt partitioning. *Chemical Geology* **117**, 167–191.

Nixon, G. T., Cabri, L. J. & Laflamme, J. H. G. (1990). Platinum-group element mineralization in lode and placer deposits associated with the Tulameen Alaskan-type complex, British Columbia. *Canadian Mineralogist* **28**, 503–535.

Noble, J. A., Jr & Taylor, H. P. (1960). Correlation of the ultramafic complexes of south eastern Alaska with those of other parts of North America and the world. In: *Petrographic Provinces, Igneous and Metamorphic Rocks*. Report of 21st International Geological Congress, Part 13. Copenhagen, pp. 188–197.

Ross, K. & Elthon, D. (1993). Cumulates from strongly depleted mid-ocean-ridge basalt. *Nature* **365**, 826–829.

Sassani, D. C. & Shock, E. L. (1998). Solubility and transport of platinum-group elements in supercritical fluids: summary and estimates of thermodynamic properties for ruthenium, rhodium, palladium, and platinum solids, aqueous ions, and complexes to 1000°C and 5 kbar. *Geochimica et Cosmochimica Acta* **62**, 2643–2671.

Sha, L. K. (1995). Genesis of zoned hydrous ultramafic/mafic–silicic intrusive complexes: and MHFC hypothesis. *Earth-Science Reviews* **39**, 59–90.

Shapiro, M. N. (1995). The Upper Cretaceous Achaivayam–Valaginian volcanic arc (Kamchatka) and kinematics of the North Pacific plates. *Geotectonics* **29**, 52–64.

Sharpe, M. R. & Hulbert, L. J. (1985). Ultramafic sills beneath the eastern Bushveld complex—mobilized suspensions of early lower zone cumulates in a parental magma with boninitic affinities. *Economic Geology* **80**, 849–871.

Shimizu, N. & Hart, S. R. (1982). Application of the ion microprobe to geochemistry and cosmochemistry. *Annual Review of Earth and Planetary Sciences* **10**, 483–526.

Slansky, E., Johan, Z., Ohnenstetter, M., Barron, L. M. & Suppel, D. (1991). Platinum mineralization in the Alaskan-type intrusive complexes near Fifield, NSW, Australia. 2. Platinum-group minerals in placer deposits at Fifield. *Mineralogy and Petrology* **43**, 161–180.

Slater, V. P., Thompson, C. K., Nettles, J., Milam, K., Stockstill, K. R., Cahill, J., Anand, M. & Taylor,L. A. (2003). An evaluation of the igneous crystallisation programs—MELTS, MAGPOX, and COMAGMAT Part II: importance of magmatic fO_2. In: *Lunar and Planetary Science XXXIV*. Houston, TX: Lunar and Planetary Institute, Abstract No. 1896.

Sobolev, A. V. (1996). Melt inclusions in minerals as a source of principal petrological information. *Petrology* **4**, 228–239.

Sobolev, A. V., Migdisov, A. A. & Portnyagin, M. V. (1996). Incompatible elements partitioning between clinopyroxene and basaltic melt based on the study of melt inclusions in minerals from Troodos, Cyprus. *Petrology* **4**, 307–317.

Sobolev, A. V., Kamenetsky, V. S. & Kononkova, N. N. (1989). New data on petrology and geochemistry of ultramafic volcanites of the Valaghinsky Range, Eastern Kamchatka. *Geokhimiya* **12**, 1694–1709 (in Russian).

Spandler, C. J., Eggins, S. M., Arculus, R. J. & Mavrogenes, J. A. (2000). Using melt inclusions to determine parent-magma compositions of layered intrusions: application to the Greenhills Complex (New Zealand), a platinum group minerals-bearing, island-arc intrusion. *Geology* **28**, 991–994.

Spandler, C. J., Arculus, R. J., Eggins, S. M., Mavrogenes, J. A., Price, R. C. & Reay, A. J. (2003). Petrogenesis of the Greenhills Complex, Southland, New Zealand: magmatic differentiation and cumulate formation at the roots of a Permian island-arc volcano. *Contributions to Mineralogy and Petrology* **144**, 703–721.

Taylor H. P., Jr (1967). The zoned ultramafic complexes of southeastern Alaska. Part 4. III. In: Wyllie, P. J. (ed.) *Ultramafic and Related Rocks*. New York: John Wiley, pp. 96–118.

Taylor H. P., Jr & Noble, J. A. (1960). Origin of the ultramafic complexes in southeastern Alaska. In: *Petrographic Provinces, Igneous and Metamorphic Rocks*. Report of 21st International Geological Congress, Part 13. Copenhagen, pp. 175–187.

Thompson, C. K., Slater, V. P., Stockstill, K. R., Anand, M., Milam, K., Nettles, J., Cahill, J. & Taylor, L. A. (2003). An evaluation of the igneous crystallisation programs—MELTS, MAGPOX, and COMAGMAT part I: does one size fit all. In: *Lunar and Planetary Science XXXIV*. Houston, TX: Lunar and Planetary Institute, Abstract No. 1881.

Thy, P., Schiffman, P. & Moores, E. (1989). Igneous mineral stratigraphy and chemistry of the Cyprus Study Project Drill Core in the plutonic sequences of the Troodos ophiolite. In: *Cyprus Crustal Study Project, Initial Report, Hole Cy-4. Geological Survey of Canada, Paper* **88–9**, 147–185.

Tistl, M., Burgath, K. P., Höhndorf, A., Kreuzer, H., Muñoz, R. & Salinas, R. (1994). Origin and emplacement of Tertiary ultramafic complexes in northwest Colombia: evidence from geochemistry and K–Ar, Sm–Nd and Rb–Sr isotopes. *Earth and Planetary Science Letters* **126**, 41–59.

Willmore, C. C., Boudreau, A. E., Spivack, A. & Kruger, F. J. (2002). Halogens of Bushveld Complex, South Africa: delta Cl-37 and Cl/F evidence for hydration melting of the source region in a back-arc setting. *Chemical Geology* **182**, 503–511.

Wood, B. J. & Blundy, J. D. (1997). A predictive model for rare earth element partitioning between clinopyroxene and anhydrous silicate melt. *Contributions to Mineralogy and Petrology* **129**, 166–181.

Yang, H.-J., Rosamond, J. Kinzler, R. J. & Grove, T. L. (1996). Experiments and models of anhydrous, basaltic olivine–plagioclase–augite saturated melts from 0·001 to 10 kbar. *Contributions to Mineralogy and Petrology* **124**, 1–18.

Zinkevich, V. P. & Tsukanov, N. V. (1992). The formation of the accretional structure of eastern Kamchatka in the Late Mesozoic and early Cenozoic. *Geotectonics* **26**, 332–343.

Zinkevich, V. P., Danyushevsky, L. V., Kamenetsky, V. S., Konstantinovskaya, E. A., Magakyan, R. G., Seliverstov, V. A. & Portnyagin, M. V. (1991). Geology and petrochemistry of the volcanic rocks from Tumrok Range (East Kamchatka). *Tikhookeanskaya Geologiya* **5**, 84–99 (in Russian).

APPENDIX

Analytical methods

Electron microprobe analyses of minerals were performed using Cameca Camebax-Microbeam (Vernadsky Institute of Geochemistry and Analytical Chemistry, RAS Moscow) and JEOL Superprobe 8200 (Max Planck Institut für Chemie, Abt. Geochemie, Mainz) electron microprobes using routine procedures. Operating conditions were 15 kV and 5–20 nA. International natural mineral standards from the Smithsonian Institution were used (Jarosevich *et al.*, 1980). The ZAF correction procedure was applied.

Trace element abundances in the clinopyroxenes (Table 4) were analysed using a Cameca IMS-4f ion microprobe (Institute of Microelectronics, RAS, Yaroslavl, Russia) following the method of Shimizu & Hart (1982). To improve beam stability and avoid mass superposition, the 10 kV O^{2-} was used instead of O^{-} as a primary beam. A primary beam current of 4 nA was focused on the sample over a spot diameter of about 25 μm. Secondary ions were collected from the imaged field of 25 μm in diameter and energy filtered using a sample offset voltage of −100 V and energy window of 50 eV (Sobolev, 1996). The analytical error was <10% for most elements present in amounts higher than 0·1 ppm and 30–50% for elements at lower concentration.

Trace element abundances in the clinopyroxenes (Table 5) were obtained using a laser ablation inductively coupled plasma-mass spectrometry (ICP-MS) system at the Max Planck Institut für Chemie, Mainz. This system includes a New Wave, Merchantek UP213 UV Nd–YAG laser coupled to a Finnigan-MAT Element-2 magnetic sector field ICP-MS system. Samples were ablated using 90 μm spots, a repetition rate of 10 Hz and a laser energy of 6 J/cm^2 in He atmosphere. The measurements were calibrated using the NIST SRM 612 and KL2-G reference glasses (Jochum *et al.*, 2000). Typical external precision is better than 4% (RSD) for most elements.